# NAVAL POSTGRADUATE SCHOOL

## MONTEREY, CALIFORNIA

# THESIS

**EFFECTS OF STRAIN PATH ON THE MICROSTRUCTURE OF ALUMINUM ALLOYS DURING EQUAL CHANNEL ANGULAR PRESSING (ECAP)**

by

Katrina M. Houston

December 2007

Thesis Advisor:     Terry McNelley
Second Reader:     Srinivasan Swaminathan

THIS PAGE INTENTIONALLY LEFT BLANK

| REPORT DOCUMENTATION PAGE | | Form Approved OMB No. 0704-0188 |
|---|---|---|
| Public reporting burden for this collection of information is estimated to average 1 hour per response, including the time for reviewing instruction, searching existing data sources, gathering and maintaining the data needed, and completing and reviewing the collection of information. Send comments regarding this burden estimate or any other aspect of this collection of information, including suggestions for reducing this burden, to Washington headquarters Services, Directorate for Information Operations and Reports, 1215 Jefferson Davis Highway, Suite 1204, Arlington, VA 22202-4302, and to the Office of Management and Budget, Paperwork Reduction Project (0704-0188) Washington DC 20503. | | |

| 1. AGENCY USE ONLY *(Leave blank)* | 2. REPORT DATE<br>December 2007 | 3. REPORT TYPE AND DATES COVERED<br>Master's Thesis |
|---|---|---|
| **4. TITLE AND SUBTITLE** Effects of Strain Path on the Microstructure of Aluminum Alloys during Equal Channel Angular Pressing (ECAP) | | **5. FUNDING NUMBERS**<br> N/A |
| **6. AUTHOR(S)** Katrina M. Houston | | |
| **7. PERFORMING ORGANIZATION NAME(S) AND ADDRESS(ES)**<br>  Naval Postgraduate School<br>  Monterey, CA  93943-5000 | | **8. PERFORMING ORGANIZATION REPORT NUMBER** |
| **9. SPONSORING /MONITORING AGENCY NAME(S) AND ADDRESS(ES)**<br>  Air Force Office of Scientific Research (AFOSR) | | **10. SPONSORING/MONITORING<br>   AGENCY REPORT NUMBER**<br>**F1ATA06058G001** |

**11. SUPPLEMENTARY NOTES**  The views expressed in this thesis are those of the author and do not reflect the official policy or position of the Department of Defense or the U.S. Government.

| **12a. DISTRIBUTION / AVAILABILITY STATEMENT**<br>Approved for public release; distribution is unlimited. | **12b. DISTRIBUTION CODE** |
|---|---|

**13. ABSTRACT (maximum 200 words)**

   Aluminum alloys AA1050 and AA6061 were processed by ECAP following either monotonic or redundant routes.  The materials were characterized by optical microscopy and orientation imaging microscopy.  Grain shape changes were analyzed in different billet planes to assess microstructure refinement mechanisms and were consistent with a proposed model.  The results demonstrate that microstructure development is not independent of processing route.  In the case of AA6061, annealing characteristics were examined to determine if the material has the requisite properties typically exhibited by a superplastic material.  Recommendations are made for future research. This work was funded in part by the Air Force Office of Scientific Research (AFOSR) under contract number F1ATA06058G001.

| **14. SUBJECT TERMS**<br>Equal Channel Angular Pressing; ECAP; Strain Path; Aluminum; Aluminum Alloys; 6061 | | | **15. NUMBER OF PAGES**<br>71 |
|---|---|---|---|
| | | | **16. PRICE CODE** |

| **17. SECURITY CLASSIFICATION OF REPORT**<br>Unclassified | **18. SECURITY CLASSIFICATION OF THIS PAGE**<br>Unclassified | **19. SECURITY CLASSIFICATION OF ABSTRACT**<br>Unclassified | **20. LIMITATION OF ABSTRACT**<br>UU |
|---|---|---|---|

Standard Form 298 (Rev. 8-98)
Prescribed by ANSI Std. Z39.18

THIS PAGE INTENTIONALLY LEFT BLANK

**Approved for public release; distribution is unlimited.**

**EFFECTS OF STRAIN PATH ON THE MICROSTRUCTURE OF ALUMINUM ALLOYS DURING EQUAL CHANNEL ANGULAR PRESSING (ECAP)**

Katrina M. Houston
Lieutenant, United States Navy
B.S., Industrial and Systems Engineering, The Ohio State University, 2000

Submitted in partial fulfillment of the
requirements for the degree of

**MASTER OF SCIENCE IN MECHANICAL ENGINEERING**

from the

**NAVAL POSTGRADUATE SCHOOL**
**December 2007**

Author:            Katrina M. Houston

Approved by:       Terry McNelley
                   Thesis Advisor

                   Srinivasan Swaminathan
                   Second Reader

                   Tony Healey
                   Chairman, Department of Mechanical and Aeronautical
                   Engineering

THIS PAGE INTENTIONALLY LEFT BLANK

# ABSTRACT

Aluminum alloys AA1050 and AA6061 were processed by ECAP following either monotonic or redundant routes. The materials were characterized by optical microscopy and orientation imaging microscopy. Grain shape changes were analyzed in different billet planes to assess microstructure refinement mechanisms and were consistent with a proposed model. The results demonstrate that microstructure development is not independent of processing route. In the case of AA6061, annealing characteristics were examined to determine if the material has the requisite properties typically exhibited by a superplastic material. Recommendations are made for future research. This work was funded in part by the Air Force Office of Scientific Research (AFOSR) under contract number F1ATA06058G001.

THIS PAGE INTENTIONALLY LEFT BLANK

# TABLE OF CONTENTS

# LIST OF FIGURES

# ACKNOWLEDGMENTS

THIS PAGE INTENTIONALLY LEFT BLANK

# I.  INTRODUCTION

Equal Channel Angular Pressing (ECAP) was first reported in 1981 by V.M. Segal, *et al.* as a materials processing method for homogenization of microstructures and later modified for property improvement [1].  The concept is to subject a material to simple shear in order to introduce large strains in repeated pressing operations leading to grain refinement to the sub-micron or even nano-scale, which will ultimately improve strength and toughness characteristics of the material.  The effect of grain refinement on strength is often described by the Hall-Petch relationship, where the increase in yield strength is inversely proportional to the square of the grain size $\left( \Delta\sigma \; \alpha \; d^{-\frac{1}{2}} \right)$ [2, 3].

In fact, ECAP has been shown to refine the microstructure to produce ultra-fine grained (UFG) materials, defined as polycrystals having grains less than ~1$\mu$m [4].  It is generally understood that the formation of high angle grain boundaries is the key to property improvements [5].   Due to the fine microstructures produced, most attention has been placed on analyzing ECAP materials with high resolution techniques, such as Transmission Electron Microscopy (TEM) [e.g., 6,7,8]. Thus, less emphasis has been placed on understanding the role of prior grains in mechanism(s) of grain refinement (which must be analyzed on a meso-scale) and the dependence on the processing route at this level.

A recent study by Garcia-Infanta, *et al.,*  of a hypo-eutectic Al-7%Si alloy with spheroidal primary aluminum grains is a notable exception to general rule of relying on only high-resolution techniques such as TEM [9].  The foundation of the analysis in that article will be elaborated upon here to include a dilute, nominally pure metal (AA1050) and an alloy with an elongated grain structure (AA6061) to test the proposed geometrically-based model of grain shape change.

## A.    ANALYSIS OF AA1050

The first part of this study will be to analyze a commercially pure (99.5%) aluminum alloy,  AA1050, with an equiaxed grain structure, that has been pressed up to two times using monotonic and redundant routes.   The microstructure will be characterized using a combination of optical and orientation imaging microscopy (OIM).   In addition, OIM will be employed to analyze texture on a meso-scale.   Empirical results will be compared with the idealized Garcia-Infanta, *et al.* model and the role of prior grains on microstructure refinement discussed [10].  Evidence may be developed to refute assertions that ultrafine grain structure development is independent of deformation path [11,12].

## B.    ANALYSIS OF AA6061

Aluminum 6061, an alloy precipitation-hardened with magnesium silicide particles, has applications in the aerospace industry.   In the T-6 condition (solution heat treated and artificially aged), AA6061 exhibits strengths between 260-310 MPa; however, it also has relatively low ductility (9-13% elongation) that inhibits forming [13].   Currently, components made of AA6061 need to be assembled with fasteners as opposed to being formed or molded.   If a processing technique is able to achieve superplasticity in this material, this could allow for the desired forming characteristics.  Low temperature (523 K) extended ductility has been reported in ECAP AA6061 billets wherein 155% elongation was attained, while at elevated temperatures (813 K), superplasticity with 280% elongation was achieved [14].   In comparison, in a spray-cast aluminum alloy 7034 ECAP processing up to 12 passes, resulting in reported grain sizes of  ~0.3 $\mu$m,  has allowed elevated temperature elongations greater than 1000% at initial strain rates at and above $10^{-2}$/s to be achieved [15].  Research has already been done for the Department of Energy to scale up ECAP to improve hot workability of AA6061 with reported success with 3-4 pressings resulting in 0.5 $\mu$m grain

sizes [16].  This holds promise for refining AA6061 grain structures by ECAP to achieve desirable formability characteristics that can be used in practice.

Thus, the second part of this study is to process AA6061 by ECAP in both monotonic and redundant routes to analyze the development of the microstructure and texture corresponding to the methods used for AA1050. Since an extruded aluminum bar with a highly elongated grain structure will be used, this will give an opportunity to study the texture evolution and mechanism of grain refinement for a material with grains having a high aspect ratio that could be compared with the model proposed by Garcia-Infanta, *et al.* [10].  Further, annealing studies will be performed to determine the recrystallization temperature to assist in directing further studies with respect to high-temperature ductility and extensive elongation (superplastic behavior).

THIS PAGE INTENTIONALLY LEFT BLANK

# II. BACKGROUND

## A. EQUAL CHANNEL ANGULAR PRESSING

In ECAP, a billet of a square or round cross section of some length is pressed though a die of some angle, $2\varphi$, with a die relief angle, $\Psi$, as shown in Figure 1 [17].
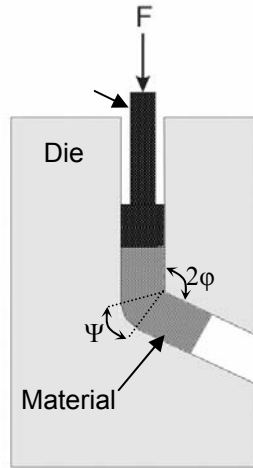


Figure 1   Generic ECAP schematic showing a billet pressed through an angle of $2\varphi$; (After: [17])

Figure 2 models the deformation of a cubic volume element upon one ECAP pressing.  Note the orientation of the coordinate axes that will be used throughout this thesis, along with configuration of the three orthogonal planes of interest.  These planes are the Flow Plane (FP) with its normal as the z-axis, the Top Plane (TP) with its normal as the y-axis, and the Cross Plane, with its normal as the x-axis (extrusion direction).  The distortion of this initially cubical element is by simple shear.  Thus, the billet's cross section remains unchanged in area, and this enables repeated pressing of the billet.
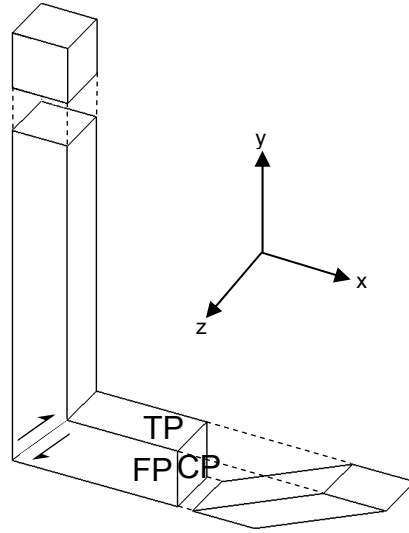
Figure 2    ECAP schematic showing deformation of a volume element and orientation of the axis and three orthogonal planes (FP=Flow Plane; TP=Top Plane; CP=Cross Plane)

## B.    PROCESSING ROUTES

Multiple pressings are usually performed (sometimes up to 12 passes, or more) via monotonic and/or redundant routes in order to refine grain structure to nano-scale dimensions [15, 18, 19]. This is facilitated by using a billet of square or round cross section that can be reinserted into the die channel. As shown in Figure 3, the monotonic routes are A and $B_A$ [20]. Monotonic routes are such that a volume element continually deforms without being returned to its original shape, as observed on the flow plane (FP). In route A, the billet is returned through the die in the same orientation every pressing (no rotation). In route $B_A$, the billet is rotated alternately 90° between pressings. In Routes $B_C$ and C, which are redundant routes, the grains are returned to their original shape every four and two passes, respectively. Route $B_C$ requires a 90° rotation in the same sense between each pressing operation, while Route C calls for a 180° rotation between pressings.
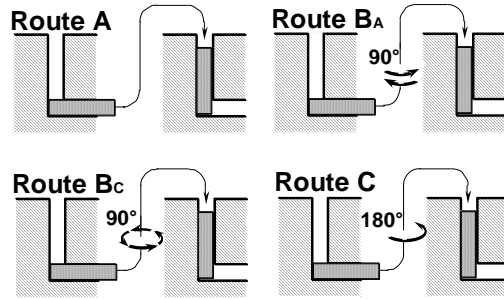
Figure 3    Monotonic (A and $B_A$) and Redundant ($B_C$ and C) routes of ECAP (From: [20])

In order to study refinement of the original grains, this study was limited to two pressings via monotonic route A and redundant route C for both AA1050 and AA6061. Figure 4 depicts the expected results of an equiaxed volume element on all three orthogonal planes for one pass and two passes, routes A and C [20,21].
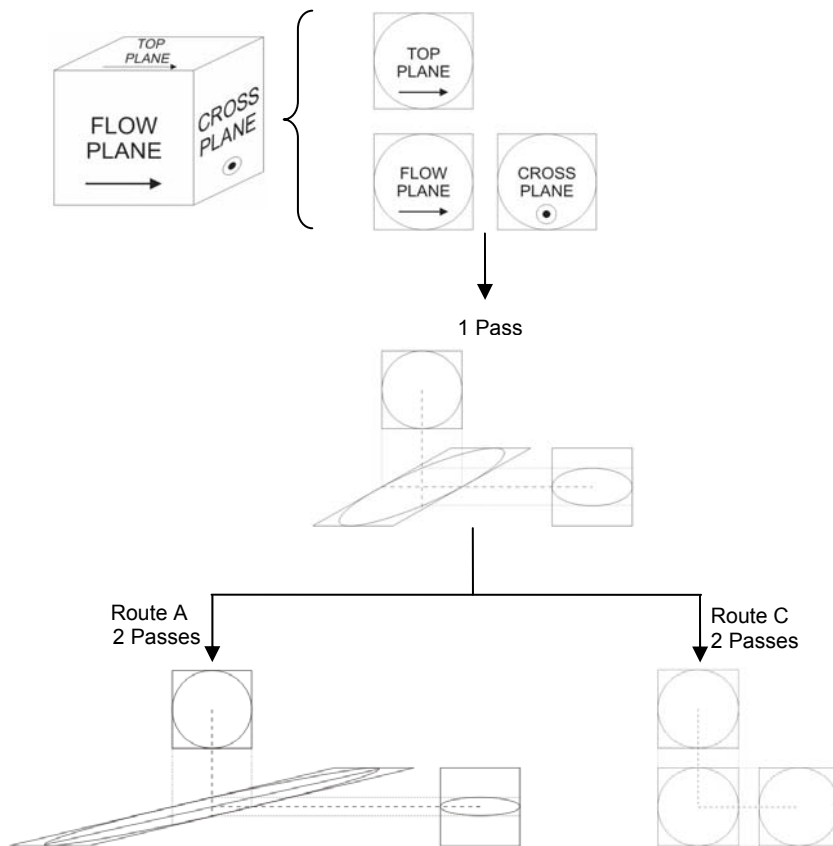


Figure 4    Idealized shearing of a cubical and spherical volume element through two passes via routes A and C

## C.    THE MODEL FOR COMPARISON

There were two models proposed by Garcia-Infanta, *et al.,* one for equiaxed grains, and one for elongated grains having aspect ratios other than unity [10].   The model is expressed by an equation that had been derived by transforming and rotating initial square and circular elements to solve for the angle of inclination, β, of the long axis of the ellipse with respect the flow plane (x-axis), as shown in Figure 5.
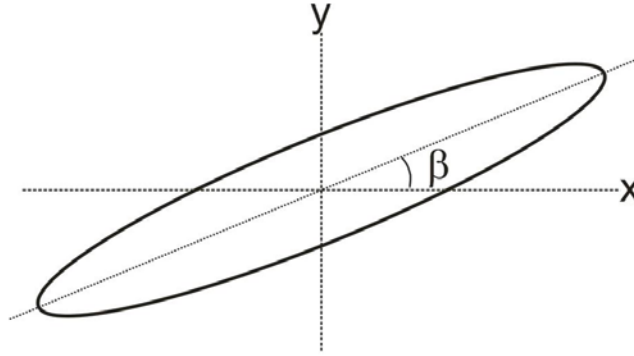


Figure 5    Ellipsoidal element showing inclination angle, β, with respect to the x-axis.

First, the shear strain, $\gamma_\varphi$, for a sharp-cornered die (ψ=0) is given by the equation $\gamma_\varphi$= 2cot (φ), where 2φ is the internal die angle [22].  For greater than one pressing operation, the shear strain is determined by multiplying the shear strain for one pass by the number of passes.  Thus, the model to determine the inclination angle, β, for initially equiaxed grains processed by monotonic Route A was derived as Equation 1 below.

$$\beta = \tan^{-1}\left[\frac{1}{2\gamma}\left(\sqrt{(2+\gamma^2)^2 - 4} - \gamma^2\right)\right]$$

Equation 1  Inclination angle, β, for initially equiaxed grains processed via Route A for a sharp-angled die and shear strain, γ (From: [10])

This equation is plotted in Figure 6 for a sharp-angled die with 2φ=90°. Note that the long-axis angle decreases with each increasing number of passes,

8

approaching zero asymptotically. Measured angles from [10] are superimposed on the graph for a shear strain up to eight (corresponding to four passes via Route A).
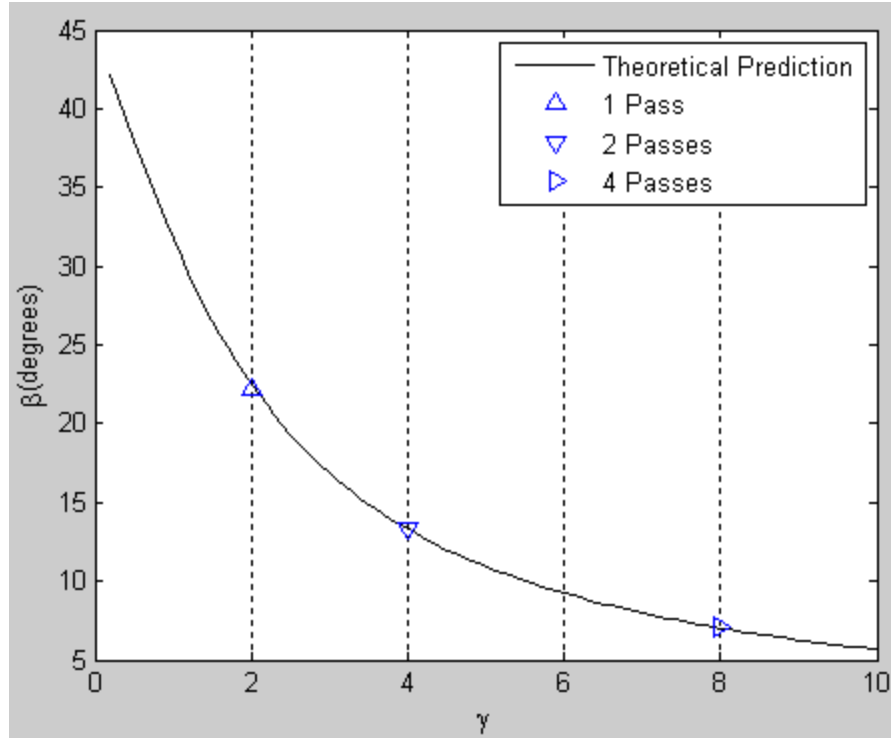


Figure 6   Theoretical prediction of grain inclination angle with respect to flow plane (x-direction) versus shear strain superimposed with empirical results achieved by Garcia-Infanta, *et al.* for initially equiaxed grains (From: [10])

Further, a model determined in similar fashion for identical die conditions was proposed for initially elongated grains with aspect ratio m=length/width as Equation 2.

$$\beta = \tan^{-1}\left[\frac{1}{2\gamma}\left(m\sqrt{\left(\frac{1+m^2+\gamma^2}{m}\right)^2 - 4} + 1 - m^2 - \gamma^2\right)\right]$$

Equation 2 Inclination   angle   for   elongated   grains   of   aspect   ratio m=length/width for a sharp angled die and a billet pressed via Route A (From: [10])

9

Figure 7 plots Equation 2 for inclination angle as a function of shear strain for aspect ratios of 0.5, 1, 5, and 10. Note that as the aspect ratio increases, the incoming grains in the billet are increasingly elongated along the die entrance channel (y-axis), and there is a significant decrease in the realignment of the major axis of the grains in the flow plane. In fact, the inclination angle first increases slightly prior to decreasing for aspect ratios near five. No empirical results have been plotted, as the model as of yet has not been tested (but will be in this study).
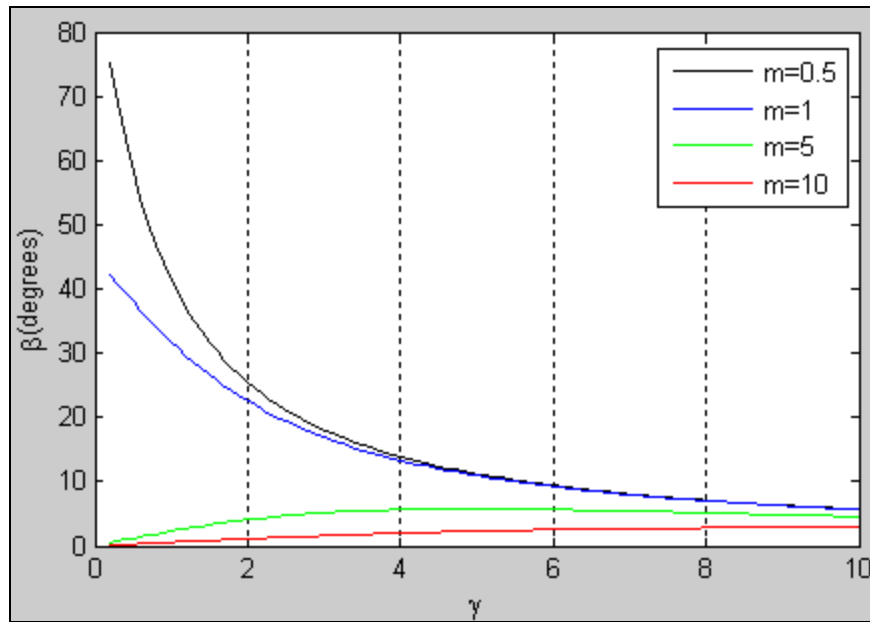


Figure 7 Theoretical prediction of grain inclination angle with respect to flow plane (x-direction) versus shear strain for initially elongated grains with select aspect ratios, m (From: [10]).

10

# III.   EXPERIMENTAL PROCEDURES

## A.   BILLET PREPARATION

AA1050 billets were cut from a rolled aluminum plate such that their length was transverse to the rolling direction.   Billet dimensions were 12.5 mm x 12.5 mm x 64 mm (~½" x ½" x 2 ½").  AA6061 billets were bandsaw cut at 64 mm (~2 ½") lengths from an extruded aluminum bar of initial dimensions of 12.5 mm x 12.5 mm (~½" x ½").

## B.   BILLET ANNEALING PRIOR TO PRESSING

To minimize stress on an unproven ECAP die, samples were annealed in a NEY 2-160 Series II annealing oven.   The commercially pure aluminum (AA1050) was annealed for five hours at 330°C followed by air cooling.   The AA6061 billets were annealed  to a "–O" condition: three hours at 415°C followed by cooling at a rate of 30°C/hr until a temperature of 200°C was reached [23] . The sample was then held at 200°C for 12 minutes followed by furnace cooling. Temperatures were monitored with an Omega Engineering Microprocessor K-type Thermocouple, Model HH21.

## C.   DIE DESIGN

### 1.   Die Design Theory

The ideal ECAP die design will impart the maximum amount of strain possible without compromising the integrity of the die or pushing a material beyond its limits for formability.  Valiev and Langdon concluded that the optimum configuration of an ECAP die consisted of an interior die channel angle, $2\varphi$, of 90°, which was also used here [4].  With no die relief angle ($\Psi$), the shear strain, $\gamma_\varphi$, imparted on the billet per pass is given by $\gamma_\varphi = 2\cot(\varphi)$ [22].  Thus, for a $2\varphi$ of 90°, the shear strain is 2.0.

In terms of die integrity, the design must be robust enough to allow for the forces it will experience during pressing.  For example, with a multi-piece design, a number of high-strength bolts are required to prevent separation of the die or relative translational movement of die parts.  Die separation is undesirable due to back extrusion of material resulting in additional frictional forces.  Translation of any pieces of the assembly can cause binding of the billet or plunger.

The forces encountered to cause such movements can be determined by modeling the billet as an incompressible fluid.  Force exerted on the top of the billet is spread over the cross sectional area of the billet (CP).  Due to Poisson's expansion, there is a Pascal's law effect that allows that pressure to be distributed equally and undiminished throughout the billet and the die walls.  Since $Pressure = \dfrac{Force}{Area}$, for a given force, the smaller the cross section of the billet, the higher the pressure that will be applied; therefore, it is important to not have too small of a cross sectional area nor make the mistake of assuming that a smaller cross sectional area along the cross plane will make pressing easier.  Further, the force exerted on the die channel walls can be modeled by taking the pressure applied at the top and multiplying it by the longitudinal area of the billet, that being the area that the die channel wall encounters.  Therefore, a longer billet will be more difficult to press and translate more stresses to the die assembly.

### 2.    Initial Die Design

The first die design was consisted of a five-piece die channel and two cover plates held together with fifteen ½" bolts and six alignment pins as shown in Figure 8.  The channel cross section was 0.5" with an interior die angle, $2\varphi$, of 90° and die relief angle, $\Psi$, of 0°.  The five interior pieces were constructed with a hardened A-2 tool steel while the one inch thick cover plates were consisted of a tougher alloy steel.

(a)                                                         (b)
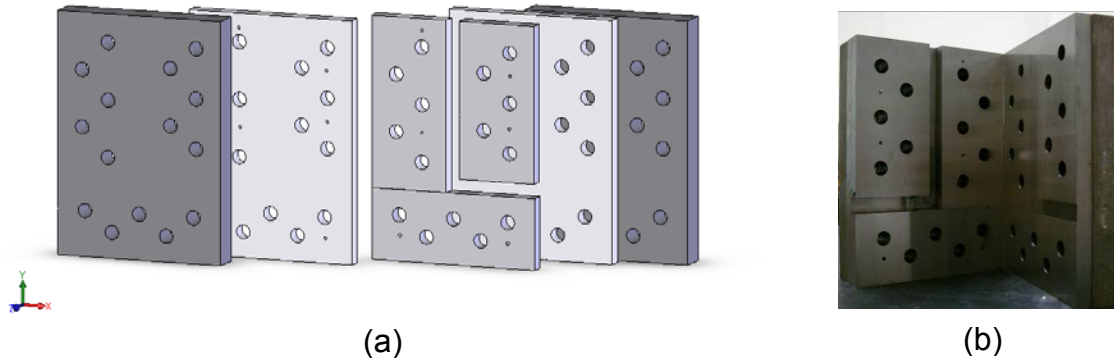
Figure 8    (a) Initial Die Design Schematic and (b) Photograph


### 3.     Initial Die Design Complications


#### a.     Die Separation

Mistakenly, the first pressing was accomplished without proper torquing of the bolts.  Grade 5 bolts were used and were hand-torqued with a wrench that had only a 7" lever arm, providing insufficient clamping force.  Figure 9 shows photographic evidence of the significant side- and back-extrusion encountered during this first pressing.



Figure 9    First pressed billet showing significant side- and back-extrusion

To mitigate this problem, a few steps were taken:

1.     Use Grade 8 Bolts (120 ksi proof strength) instead of Grade 5 bolts (85 ksi proof strength).

2.     Determine the torque that should be applied to each bolt.

3.     Determine the maximum allowable load to prevent die separation.

13

### b.    *Torque Calculations*

The proper torque was determined using Equation 3 [24]:

$T = KdF_i$

where

$K = $ Torque Factor $\approx 0.20$ in most cases

$d = $ Nominal Major Diameter $= 0.5"$ for $\frac{1}{2}''$ bolts

$F_i = $ Preload $= \begin{cases} 0.75\,F_p \text{ for reused conditions} \\ 0.90\,F_p \text{ for permanent conditions} \end{cases}$

$F_p = $ Proof load $= A_t S_p$

$A_t = $ tensile stress area $= 0.1599\,\text{in}^2$ for $\frac{1}{2}''$ UNF bolts

$S_p$=minimum proof strength=120 ksi for Grade 8 bolts

Equation 3  Torque Calculation

To be conservative, reuse conditions are assumed.   Applying appropriate unit conversions, this yields an applied torque of 120 ft-lbs.

Upon preparation for the next pressing, the bolts were torqued down with an Armstrong torque wrench to 120 ft-lbs.   Complications in die alignment resulted in a need to disassemble the die prior to the next pressing operation; however several of the bolt threads galled and one nut seized onto the bolt.  This caused a revisitation of the torque calculations.  Upon a closer look, although Shigley recommends that a Torque Factor, K, of 0.20 in most cases, he recommends that it be reduced to 0.18 for lubricated bolts, and 0.16 for cadmium plated bolts [24].   Therefore, the cadmium plating alone would reduce the required bolt torque to 96 ft-lbs.  Accounting for a 10% reduction with lubrication, a new bolt torque was determined to be approximately 86 ft-lbs.

Indeed, this eliminated side-extrusion of the billets between the die pieces, however, upon each disassembly that was made, lubrication was still found to have seeped between the die plates.

### c. Clamping Force Calculations

With a pressing machine capable of a 50,000 pound load, it was of interest to know if our die was capable of handling such a load. Bolt failure and die separation both had to be considered, using Shigley as a reference once again [24].

| | | |
|---|---|---|
| Bolt size (d) | 1/2 | in |
| Maj. Dia. Area ($A_d$) | 0.1963 | $in^2$ |
| Tensile Stress Area ($A_t$) | 0.1599 | $in^2$ |
| Modulus of bolt (E) | 30,000,000.00 | psi |
| Grip length (l) | 3.38 | in |
| Unthreaded length($l_d$) | 3 | in |
| Threaded length ($l_t$) | 0.38 | in |
| $k_b = \dfrac{A_d A_t E}{A_d l_t + A_t l_d}$ | 1,702,215.52 | lbs/in (bolt stiffness) |
| $k_m = \dfrac{0.577 \pi E d}{2\ln\left(5\dfrac{0.577l + 0.5d}{0.577l + 2.5d}\right)}$ | 11,013,900.85 | lbs/in (member stiffness) |
| C=kb/(km+kb) | 0.13 | (fraction bolt load) |
| 1-C | 0.87 | (fraction member load) |

Table 1    Joint Stiffness and Member Stiffness Calculation Summary

Now, it is of interest to determine the factors of safety against bolt failure and joint separation. These are determined by the following equations, where $n_j$ is the factor of safety against joint separation and $n_b$ is the factor of safety against bolt failure:

$$n_j = \frac{F_i}{P(1-C)}$$

$F_i$ = preload (determined from previous calculations to be 14,391 lbs)

$P$ = external tensile load ($= 26,667$ lbs for a maximum applied load of 50,000 pounds, cross plane sectional area of 0.25 in$^2$, and billet length of 4 in; 15 bolts)

(1-C)= fraction of member load

$$n_b = \frac{S_p A_t - F_i}{CP}$$

$S_p$ = bolt proof strength (120,000 psi)

$A_t$ = tensile stress area (0.1599 in$^2$)

$F_i$ = preload (determined from previous calculations to be 14,391 lbs)

$P$ = external tensile load ($= 26,667$ lbs, as before)

$C$ = fraction of bolt load

Equation 4  Safety Factors against Joint Separation and Bolt Failure

For both cases, a factor of safety of at least 1 is required.  The bolt factor of safety is 1.3, meaning that the bolts should be able to handle the full pressing load in the current load cell.  However, the factor of safety against joint separation is only 0.62, meaning failure would occur below maximum load in terms of joint separation resulting in side extrusion of the billet.  Further calculations determine that the bolt preload required to prevent joint separation is 23.4 kips while each bolt has been determined to apply 14.4 kips.

A different perspective to the analysis can be taken as follows:  for what billet configuration and load combination can die separation be prevented?  That is to say, at what point is the bolt preload exceeded that induces a residual compressive stress?  At this point, the net force on the die members will be zero.  Figure 10 depicts this information graphically for select billet configurations.  Having a cross section of 0.25" on a side is clearly undesirable, as discussed previously.  Increasing billet side dimension to 0.75" will allow us to have a billet length of 3.75" and apply a force up to 50,000 pounds; however, it is desirable to continue with our existing design of 0.5", if possible.

Force on Die Members vs. Satec Force (F on die<0 Desirable)
1/2" Bolts
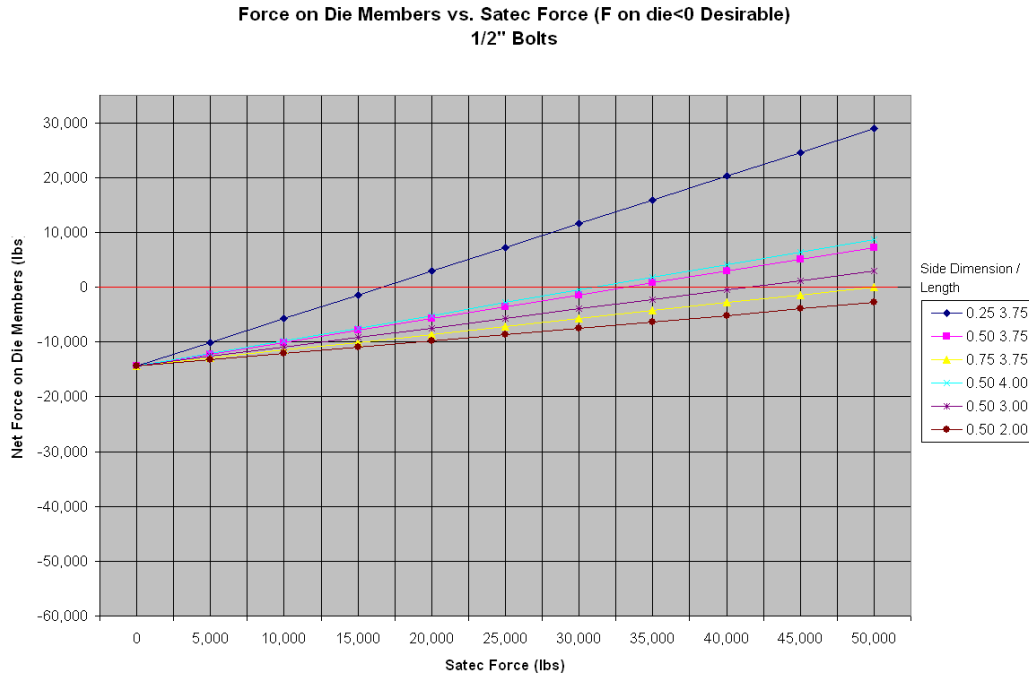
Figure 10   Plot of net force on die members versus applied force for various
billet configurations

While a billet length of 2" will clearly allow us to press safely, it is not practical for multiple pressings due to frictional effects that cause non-uniform deformation at the very front of the billet and an angular exit tail.  A billet length of 4" allows us to go up to approximately 31,000 pounds, while a 3" billet allows for 41,000 pounds.  One should note that these results are for a safety factor of 1.

### d.       *Die Plate Relative Translational Motion*

Once the clamping force issue was resolved, pressing operations resumed.  A billet of AA1050 was successfully pressed with no complications, so a following AA1050 billet was inserted and pressed with the first one still in the die.  With greater billet surface area contacting the die, frictional forces increased significantly, requiring a higher pressing load.  Due to increased forces required, this put greater stresses on the die.  Slight unloading of the die pieces allowed for extrusion of the lubrication in between the die pieces.  This reduced the friction on already smooth surfaces of the die assembly.  The tolerances on the bolts

and alignment pins were insufficient to prevent rotation of the top two central die pieces when the plunger was close to the bottom of the channel. This rotation prevented the plunger from extracting without die disassembly. Further, this rotation separated the plates laterally, allowing back extrusion to occur past the plunger. This led to a significant increase in friction, resulting in higher forces applied to press the sample, which spiraled the problem of rotation. Figure 11 shows a photograph of a failed pressing due to die piece rotation and the relative motion encountered.
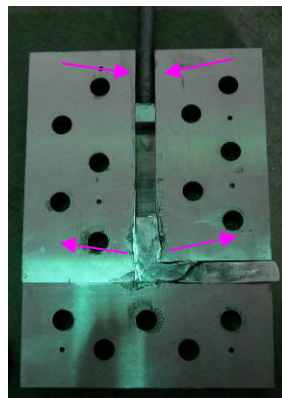


Figure 11   Directions of relative movement of die pieces

With adding C-clamps as reinforcements, and die disassembly after each pass, pressing continued, now with AA6061-O until plunger failure occurred due to buckling at 174,000 N (39,000 pounds). This mode of failure to the plunger became the new limiting factor to the maximum load. Since such loads should not be required under normal conditions with no back-extrusion caused by plate rotation, a new die design was in order.

Figure 12   Plunger Failure

### 4.      Die Redesign

Die redesign had to consider two important issues:  1) Die piece rotation, and 2) Die separation.  Inspired by Garcia-Infanta's design, the new construction consisted of four pieces:   two for the die channel and two for a carrier surrounding the die channel.   By fitting a two-piece die channel within a die carrier to hold the channel rigid, this completely eliminated relative translational motion of the pieces.  Further, the die channel was designed to sit out of the die carrier by 0.001" to focus clamping forces on the die channel.  Further, the new design incorporated 21 bolts to increase the clamping force (allowing for a factor of safety of 1.23 for joint separation at a maximum load of 50,000 pounds). Figure 13 shows a schematic of the new ECAP die assembly.
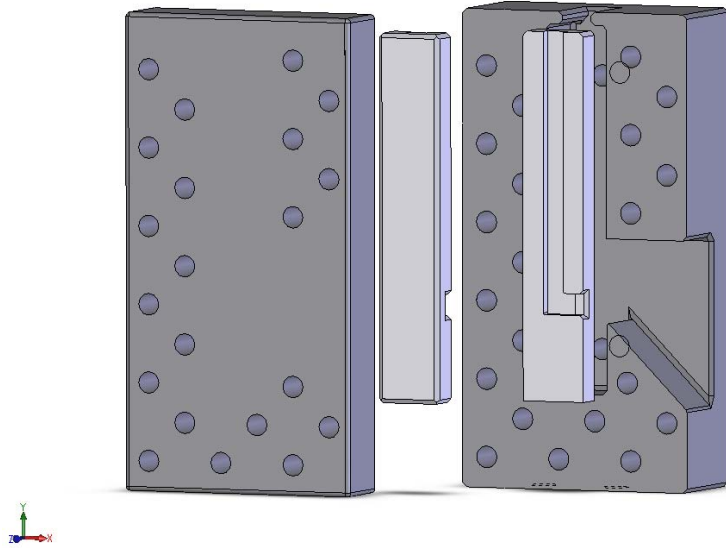
Figure 13   Redesigned ECAP Die

This die carrier design also allow for interchangeable channels, allowing pressing at a die angle up to 135°.  The main die carrier houses the entire channel while the cover plate is machined flat, allowing for more efficient production.  The channel fits snug within the carrier, so two threaded holes on the outside of the channel were tapped to allow bolts to push the channel out for disassembly.

## 5.    New Die Design Complications

The new die Figure 14 was received with nine bolt holes instead of 21 resulting in a factor of safety against joint separation based on the previous model of 0.53, lower than the previous 0.62.  However, instead of the holes being drilled through, they were threaded, theoretically allowing for shorter bolts, less stretching of those bolts, and more threads to grip.  Upon pressing, some die separation was observed by samples having a clear seam down the center along the top and bottom reflecting where the die halves come together.

Figure 14   Photograph of new ECAP assembly on Satec pressing machine

Although the negative effects in AA1050 were minimal, pressing of AA6061-O resulted in back extrusion past the plunger (Figure 15) and two similar failures of the die channels (Figure 16 and Figure 17).



Figure 15   Evidence of back-extrusion on the plunger
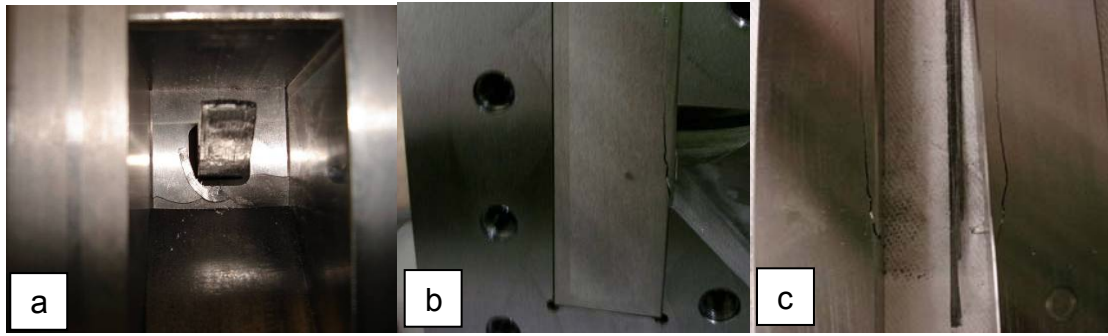
Figure 16   First channel failure.   a) Extrusion of aluminum through cracks below exit channel; b) side-view of channel failure; c) failure of both halves of die channel



Figure 17   Second channel failure

## 6.      Recommendations for Modification

A-2 tool steel in all its strength is a very brittle material.  Therefore, stress concentrators, such as corners necessitated by the ECAP process are natural crack initiation sites.   This can be mitigated by inducing a larger residual compressive stress by adding more bolts and/or using larger diameter bolts, such as ¾".  In a new die carrier, if eleven ¾" bolts were used, this would result in a factor of safety against joint separation of 1.58 and bolt failure of 1.9.  These high values are extremely desirable.  Again, inducing this larger compressive stress

may also mitigate stress concentrations at the corners.  Also, it may be more prudent to consider a tougher steel for the die channel, as opposed to the A-2 tool steel currently used.

Further, it may be desirable for 90° pressing to have a more solid channel with a straight exit.  The previous design with the angled exit may have weakened this area, allowing the channel to expand in this region, which may explain the similarity in the cracks in both failures.  Figure 18 depicts the redesigned die carrier with the existing 90° die channel.
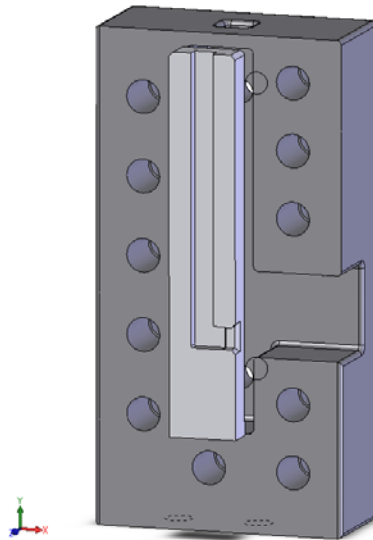


Figure 18   Redesigned die carrier

Finally, depending on the amounts of strain hardening encountered upon further pressings, it may be necessary to reduce the amount of strain per pass by increasing the die angle up to $2\varphi=135°$ or pressing at elevated temperatures. Chaudhury *et al.* have reported a hardness plateau at three to four passes [16].

## D.    ECAP PRESSING

Pressing was performed at room temperature using a SATEC Unidrive, Model 2OUD coupled with a  SATEC  MATS II Testing System at a rate of 10mm/min.  Loads were monitored with the MATS II NuVision II version 4.04 software.  Peak loads are summarized in Table 2.

| Material/Pass | Date | Satec Load (kN) | Material/Pass | Date | Satec Load (kN) |
|---|---|---|---|---|---|
| ORIGINAL DIE DESIGN | | | NEW DIE DESIGN | | |
| 1050 1P | (7/19/07) | 38.6 | 1050 1P | (10/26/07) | 41.1 |
| 1050 1P | (7/19/07) | 61.6 | 1050 1P | (10/26/07) | 54 |
| 1050 1P | (8/26/07) | 35.8 | 1050 2C | (10/26/07) | 58 |
| 1050 1P | (8/26/07) | 47.4 | 1050 2A | (10/29/07) | 74.5 |
| 1050 2A | (8/28/07) | 63 | 6061 1P | (10/30/07) | 74.7 |
| 1050 2C | (8/28/07) | 52.8 | 6061 1P | (10/30/07) | 76.6 |
| 6061 1P | (9/2/07) | 78.6 | 6061 1P | (10/30/07) | 68.7 |
| 6061 1P | (9/2/07) | 66 | 6061 2C | (10/31/07) | 96* |
| 6061 2A | (9/2/07) | 174* | 6061 1P | (11/2/07) | 96.5 |
| | | | 6061 1P | (11/2/07) | 108* |

\* Denotes failed/incomplete pressing to plunger or die failure

Table 2    Summary of peak loads achieved during ECAP

## E.    SAMPLE PREPARATION

### 1.    Sample Sectioning

Billets were sectioned on three planes to reveal the central structure using a Buehler Isomet low speed saw with a Buehler Diamond Wafering Blade, Series 15HC using copious lubrication to prevent frictional heating.  Samples used for optical and orientation imaging microscopy were allowed to be as small as 6mm x 12mm (~¼" x ½"), given that the center of the plane was able to be analyzed.

### 2.    Grinding and Polishing

Grinding was performed using successively finer grit papers, namely P400, P1200, P2400, then P4000.  Most effective polishing was achieved when

each sample was ground on each step from one to two minutes by hand with periodic 90 degree rotations and frequent rinsing of the sample and grinding paper under a high-velocity stream of water using a hose connector nozzle on the faucet.  Each step was considered complete when one or two strokes with extremely light pressure completely removed the previous perpendicular scratches.

Polishing was carried out using an Ecomet 3 Variable Speed Grinder-Polisher operating between 190-240 rpm.  A black fine nap pad was used in conjunction with water-based 6µm, 3µm, and 1µm Buehler MetaDi Monocrystalline Diamond Suspensions successively.  Care was taken to restrict each pad to its respective solution to prevent contamination.  Before and after each use, each pad was rinsed with a high velocity stream of water to remove any contaminating particles that could scratch the samples.  When rinsing prior to polishing, excess water was removed by applying pressure to the pad with the side of a hand while the wheel was spinning.  These steps were necessary to prevent the sample from getting scratched from an excessively dry pad or polishing to take excessively long from the solution being too dilute.

Samples were then electropolished with an Electromet 4 Electoropolisher.  Samples used for both OIM analysis and optical micrographs used a solution consisting of 800 ml ethanol, 140 ml distilled water, and 60 ml perchloric acid (60% concentration) chilled to 15°C with the electropolisher operating at 30 volts for 15 seconds [25].

### 3.    Etching

Finding the best etching solution to reveal the grain structure of 1050 aluminum proved difficult.   Several solutions referred to in the Materials Handbook, Volume 9 were attempted, including Tucker's, Poulton's, Barker's and Keller's reagents and a HF etch; however these proved unsuccessful [26]. Poulton's reagent showed the most promise, but was quick to overetch the samples for optical microscopy.  However, a clear grain structure could be seen

with the naked eye.  Thus, a diluted version of Poulton's reagent was used consisting of 10% HF, 10% HCl, and 25% $HNO_3$ in a balance of distilled water.  It was critical to use this etchant chilled, else it would quickly overetch the sample as well.  At 15°C, it was necessary to etch each sample for 2 ½ minutes for optimum results in AA1050, and 1 minute for AA6061.  Each sample was rinsed with water and dried prior to further analysis.

## F.    METHODS OF ANALYSIS

### 1.    Optical Microscopy

A Nikon Epiphot 200 Inverted Metallurgical Microscope coupled with NIS Elements F 2.30, SP2 imaging software was used to analyze macroscopic grain structure on three orthogonal planes.  Multiple images of each sample of were taken near the center of each orthogonal plane at 2.5x and 10x while carefully preserving sample orientation to ensure accurate angular measurements. Additional micrographs of AA6061 were taken at 20x and 50x magnifications.

### 2.    OIM Analysis

Optical Imaging Microscopy Analysis (OIM) utilized a Topcon SM-510 Scanning Electron Microscope (SEM) operating at 15kV with a $LaB_6$ filament and equipped with an EDAX-TSL OIM system.  To illustrate microstructure at different levels scan areas were varied at different magnifications. The step size was accordingly adjusted to vary between 0.1 $\mu$m to 2 $\mu$m. TSL OIM Analysis 4.6 software was used to analyze and clean up the data [27].  The image clean-up procedure included:

1.    grain dilation with grain tolerance angle of 5° and a minimum grain size of 2 pixels

2.    grain confidence index (CI) standardization with grain tolerance angle of 5° and minimum grain size of 2 pixels

3.    Neighbor CI correlation with a minimum CI of 0.05.

## G.   ANNEALING STUDIES

Annealing studies were performed on one-pass AA6061 samples using a NEY 2-160 Series II annealing oven.  Temperatures were monitored with two Omega Engineering Microprocessor K-type Thermocouples, Model HH21, one beneath the ceramic platform, and one above that touched the sample.  The first study held the oven at 450°C and altered annealing times.  The one-pass AA6061 billet was sectioned into 12 mm tall x 6 mm wide x 1.5 mm thick (~½" x ¼" x 1/16") samples to reveal the flow plane.  Due to the small size of these samples, they were placed on a 12 mm x 12 mm x 51 mm long (~½" x ½" x 2") piece of AA6061 cut from bar stock.  Annealing time began once the temperature touching the sample reached within 5°C of the desired temperature, i.e., 445°C. Table 3 summarizes these warm-up times and the annealing time for each sample.

| Sample # | Warm-up time (min:sec) | Annealing time (min) |
|---|---|---|
| 1 | 10:26 | 6 |
| 2 | 10:51 | 12 |
| 3 | 10:45 | 30 |
| 4 | 12:36 | 60 |
| 5 | 11:15 | 120 |

Table 3    Annealing study at 450°C

The second annealing study on the one-pass AA6061 came from a billet processed with the new die design.  These samples were cut 12 mm tall x 6 mm wide x 6 mm thick (~½" x ¼" x ¼"), but were still placed on a larger piece of aluminum stock during annealing.  Again, the flow plane was of interest.  Table 4 summarizes the annealing temperatures and warm up times for this one-hour study.

| Sample # | Warm-up time (min:sec) | Annealing Temp (°C) |
|----------|------------------------|---------------------|
| 1        | 6:18                   | 250                 |
| 2        | 7:01                   | 350                 |
| 3        | 9:27                   | 450                 |

Table 4     1-Hour Annealing Study

Annealed samples were characterized for their grain sizes using Orientation Imaging Microscopy (OIM).

# IV. RESULTS, DISCUSSION, AND CONCLUSIONS

## A. AA1050

### 1. Optical Micrographs

On the left-hand side in Figure 19, optical micrographs from the three orthogonal planes for a representative annealed sample prior to pressing are shown, while corresponding micrographs following one ECAP pass are shown to the right. The annealed sample (left column) is considered representative. What these micrographs show is a clearly equiaxed grain structure. The alignment of the insoluble constituent particles gives an indication of the original rolling direction of the plate from which the billets were cut; billet longitudinal axes were transverse to the plate rolling direction.

The right column of Figure 19 depicts typical micrographs of the one-pass sample. Following the model from Figure 4 and the model described by Garcia-Infanta, *et al.*, the expected elongation and 22.5° tilt of the long axis of the now-elliptical grains with respect to the extrusion direction (x-axis) is clearly seen on the flow plane [10]. Also, as expected, the grains continue to be equiaxed on the top plane with an additional feature of shear bands seen in some grains. On the cross plane, the compression of the grains may be seen, but these data are not conclusive. Shear bands are also seen on the cross plane.

Thus, optical micrographs have confirmed the theoretical model of one-pass ECAP of an initially equiaxed grain structure.

| Annealed* AA1050 | | 1 Pass AA1050 |
|---|---|---|
|  | Flow Plane  |  |
|  | Top Plane  |  |
|  | Cross Plane  |  |
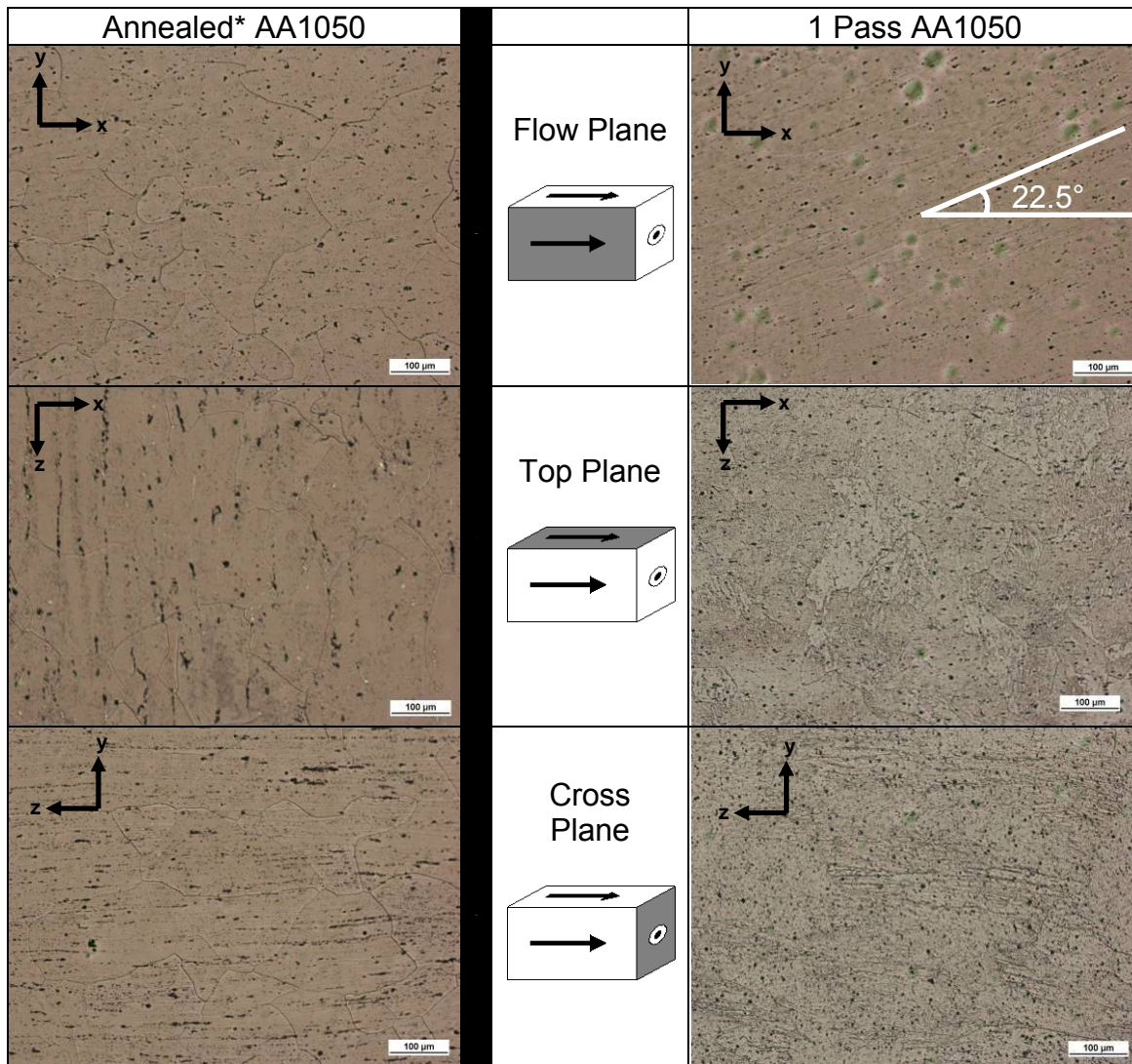
*For Annealed 1050, each image is representative of the plane the sample will become upon pressing.

Figure 19  Optical micrographs of AA1050  in the annealed condition and one- pass for the three orthogonal planes

Recall in Route A, a sample is pressed repeatedly with no rotation of the billet.  The optical results of this monotonic pressing for two passes are depicted in Figure 20.  Again, the grains appear to have sheared according to the model. An angle of 13° with respect to the extrusion direction (x-axis) was measured on the flow plane.  Due to increased distortion of the grains, resolution of an

equiaxed structure along the top plane has become difficult.   An increased number of shear bands compared to one pass is clearly distinguished.   Again, the shear bands can be seen along the cross plane, but the compression of the grains is unclear, but may be speculated.

In the redundant Route C, the sample is rotated 180° between pressings. This, theoretically, results in a return of the grains to their original shape.   The last column of Figure 20 shows this new grain structure on all three planes.   The grains on the flow plane have become relatively equiaxed, although the particles form a pattern that flows opposite to the extrusion direction, presumably due to friction affects along the die wall.   For comparison to the equiaxed original structure, in Figure 21 the notional flow plane is juxtaposed with the flow plane of the two-pass Route C flow plane.   For further clarification, the grain boundaries were enhanced with the pen function on a tablet PC.   This figure shows clearly the return to an equiaxed grain structure that fits the theoretical model.   The top plane continues to be equiaxed once again, with an increase in shear bands forming relative to one pass.   The shear bands in the cross plane make the grain structure difficult to resolve; however, the grains definitely do not appear compressed and there is evidence of an equiaxed grain structure.   The juxtaposition of the cross plane micrographs of two-pass route A and two-pass route C make the compression of the grains in Route A more evident.

With optical micrographs on all three planes that validate the theoretical models of ECAP pressing though one-pass and two-passes routes A and C, there is clear evidence that the prior grain boundaries play a role in the microstructure evolution.

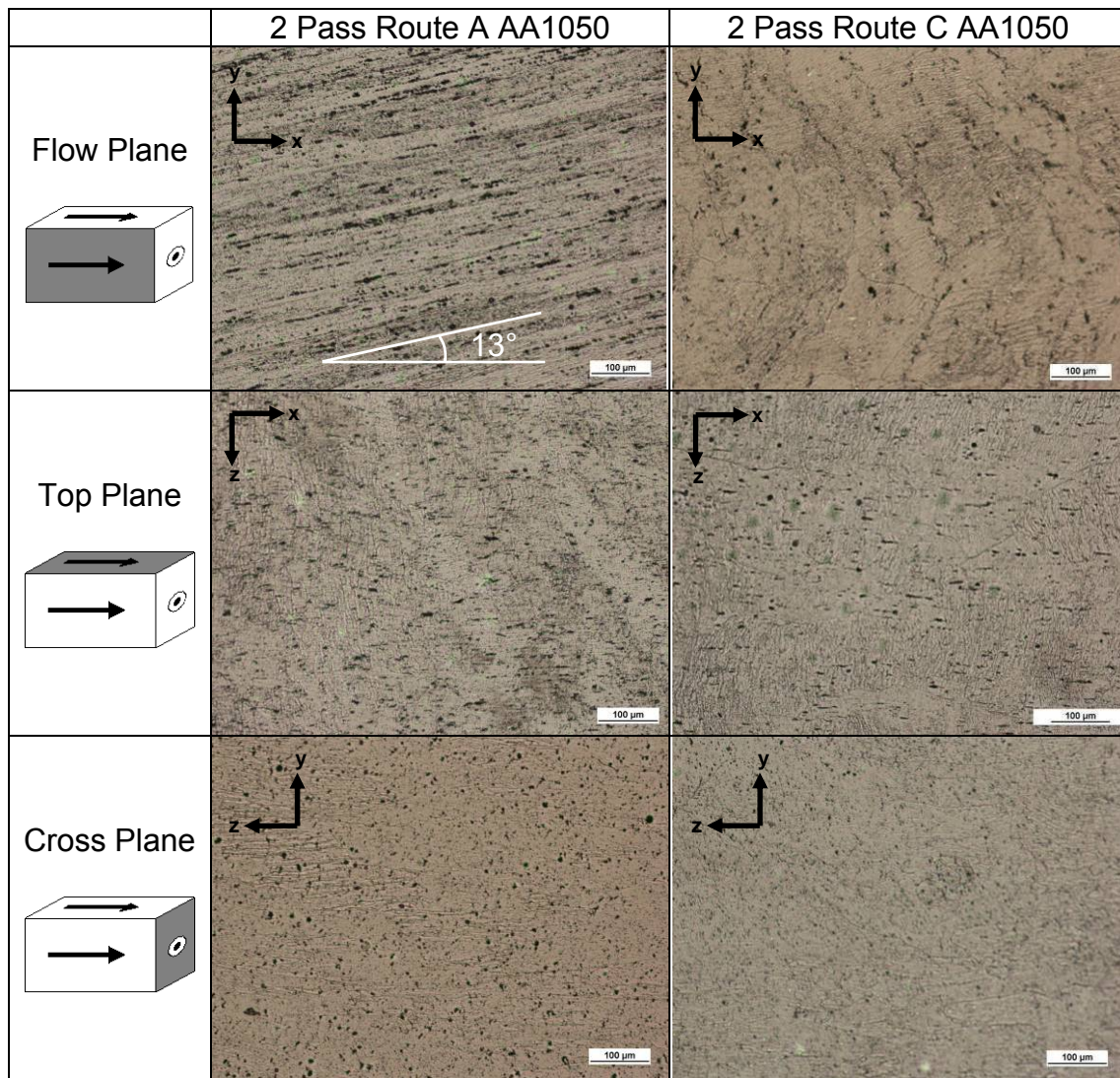| | 2 Pass Route A AA1050 | 2 Pass Route C AA1050 |
|---|---|---|
| Flow Plane |  |  |
| Top Plane |  |  |
| Cross Plane |  |  |

Figure 20    Optical Micrographs on three orthogonal planes for monotonic route A and redundant route C
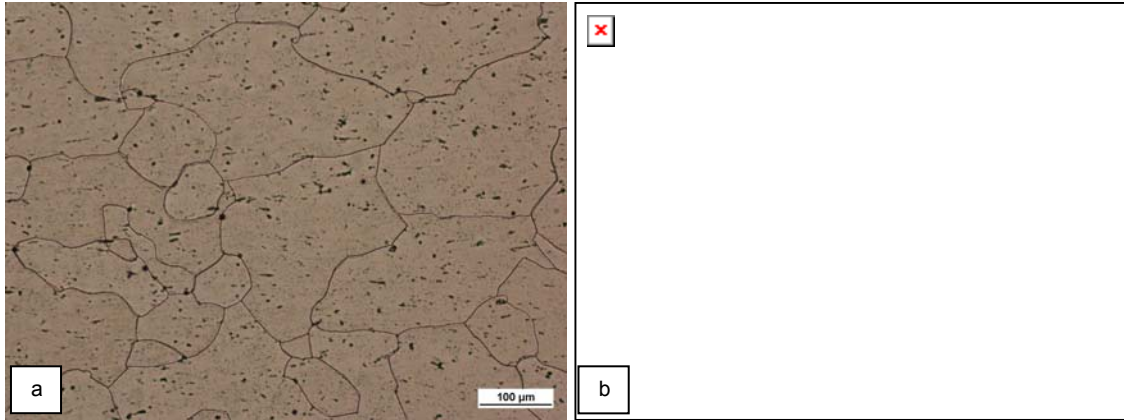
Figure 21   Enhanced grain boundaries for comparison in (a) annealed, unpressed material, and (b) two passes route C

## 2.    Orientation Imaging Microscopy Results

Figure 22 shows a representative OIM image of annealed AA1050 material prior to pressing.  This could reflect either the flow plane or the top plane and will be used for comparison with both planes upon pressing of the material. Notice that the grain boundaries are sharp, with no color variation in the grain interiors.  This indicates lack of dislocation structures.  High angle boundaries (>15°) are marked by black lines in the figure.  The presence of black lines within a grain likely indicates the presence of constituent particles.
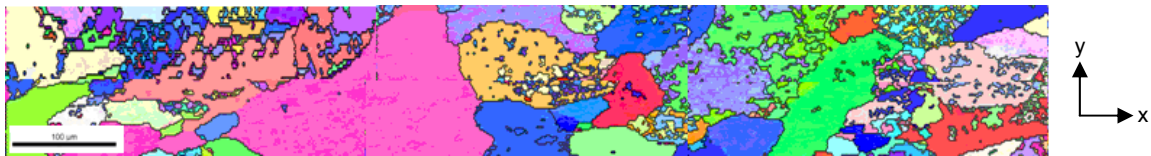


Figure 22   Representative OIM image of annealed, unpressed AA1050 flow plane/top plane

Figure 23 summarizes the OIM results at similar magnifications for the flow plane for one and two pressings via routes A and C.  Once again, an angle of 22.5° is measured for the grain orientation for the one-pass sample on the flow plane while an angle of 13° is determined for the two-pass route A sample.  Both results are consistent with the optical results (see Figure 19 and Figure 20) and

33

the Garcia-Infanta, *et al.* theoretical model [10].  It should be noted that the original grains are becoming thinner and more elongated with each pass while the grain boundaries become more distorted with each pressing, but the original grains, albeit sheared, can still be distinguished.

For two passes via Route C, as in the optical images, OIM imaging reveals an approximate return of the grain structure to a more equiaxed condition, as shown in Figure 23.  Overall, the grain boundaries can still be distinguished but are distorted due to the induced strain causing in interaction of the grain boundaries with the dislocation structures and shear bands.
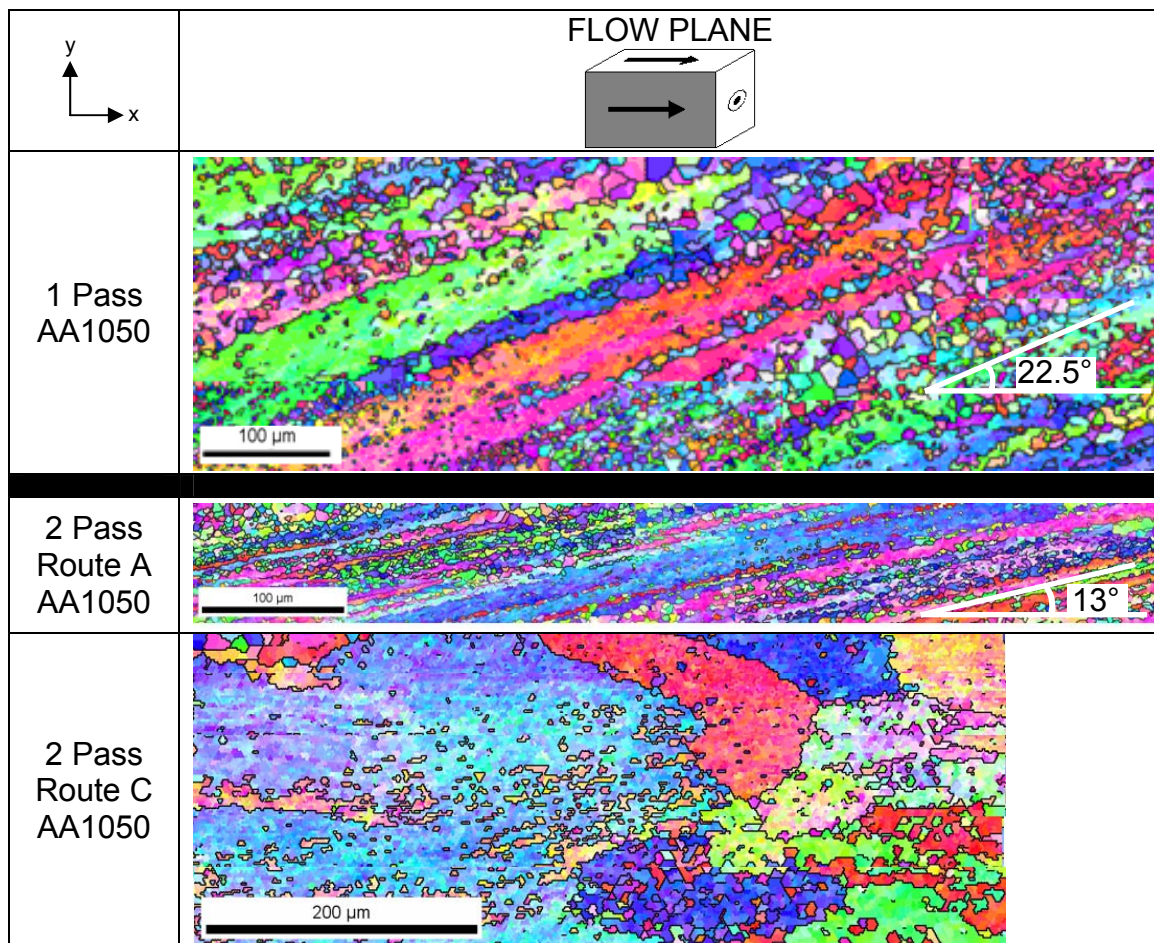


Figure 23   A1050 OIM Flow Plane Results Summary

34

Results of OIM imaging of the top plane for one-pass and two-passes via routes A and C are summarized in Figure 24. In all cases, the grains appear to retain their original shape. Increased number of pressings via routes A and C once again disrupt the clarity of the grain boundaries. The image of the two-pass, route A sample appears small due to difficulty in capturing an image with the large amount of induced strain. Thus, step size had to be reduced to obtain a clear image with a satisfactory confidence index, and the picture was adjusted to allow for a micron bar comparable to the one-pass and two-C, samples. In the two-C sample, there is a blue-violet (also enhanced with a tablet pen) spearhead-shaped grain where the deformation banding can be seen which is similar to that seen in the optical images (see Figure 19 and Figure 20). So, in addition to the grain boundaries being broken up, the grain itself is becoming more disoriented internally due to the shear bands.
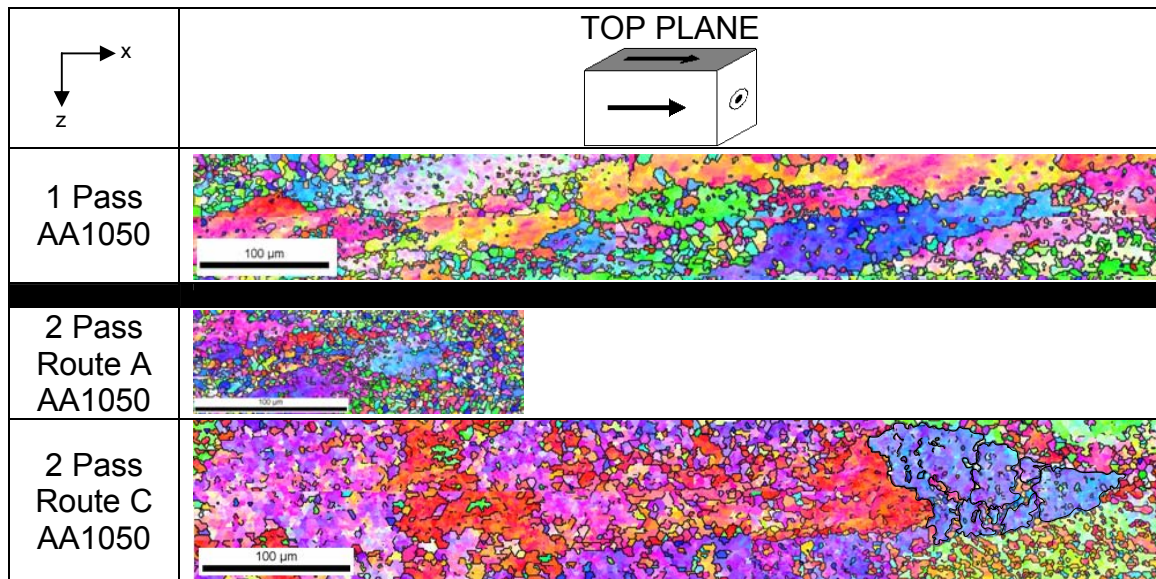


Figure 24   AA1050 OIM Top Plane Results Summary

There have been mixed results as to which processing route produces more high-angle grain boundaries that give desired properties. For example, Salem, *et al.* [28] reported that Bc was more effective in aluminum than route C

35

(in general, much is said about the preferred equiaxed structure produced by Bc [6,29,30]); however, Gholinia, *et al.*, [31] concluded that route A was best for an aluminum alloy, followed by both B routes, with the least effective being route C in terms of producing a submicron grain structure.

Figure 25 helps to illustrate the point as to why it is necessary to look on a meso-scale to understand the underlying mechanisms of grain refinement that occur during ECAP in order to determine the best processing route.  As was stated previously, most studies focus on high-resolution imaging to determine grain size, because it is nano-crystalline structures that many researchers are aiming for.  Figure 25 presents a comparison of image-quality  maps for samples processed by two passes following either route A or route C.  A comparison of these images suggest little difference in the local sense of shear, although finer subgrains are apparent in the material processed by route C.  While these maps are representative, there is considerable variation throughout each sample and it would be difficult to distinguish these samples and identify processing strain path based on such higher-resolution images.
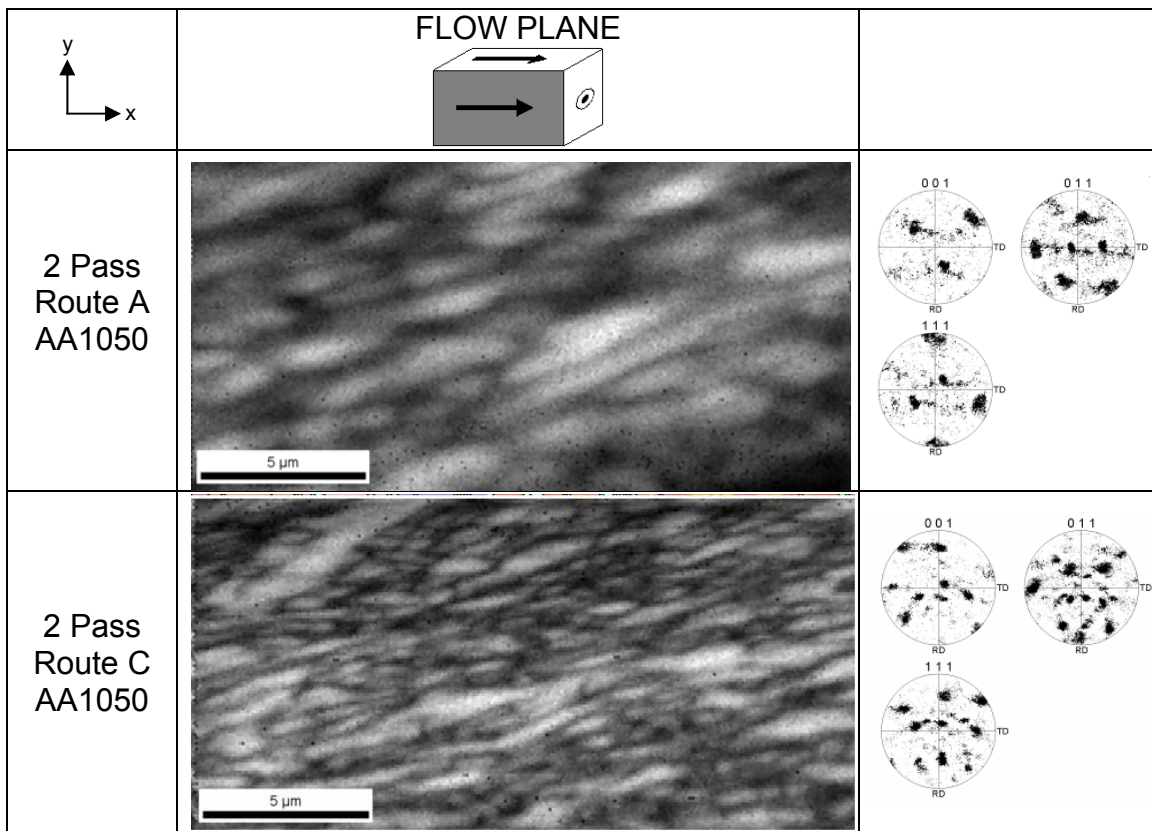
Figure 25   Inverse Pole Figure and Image Quality Maps for two passes via routes A and C

## 3.      Conclusions and Suggestions for Further Research on AA1050

AA1050 has shown that grains up to two passes via routes A or C change shape as in the Garcia-Infanta, *et al*. model, and results are summarized in Figure 26.    These results are a stepping stone for understanding the mechanisms of grain refinement and the role played by strain path.  The role of alloying constituents on grain refinement mechanisms should also be investigated.
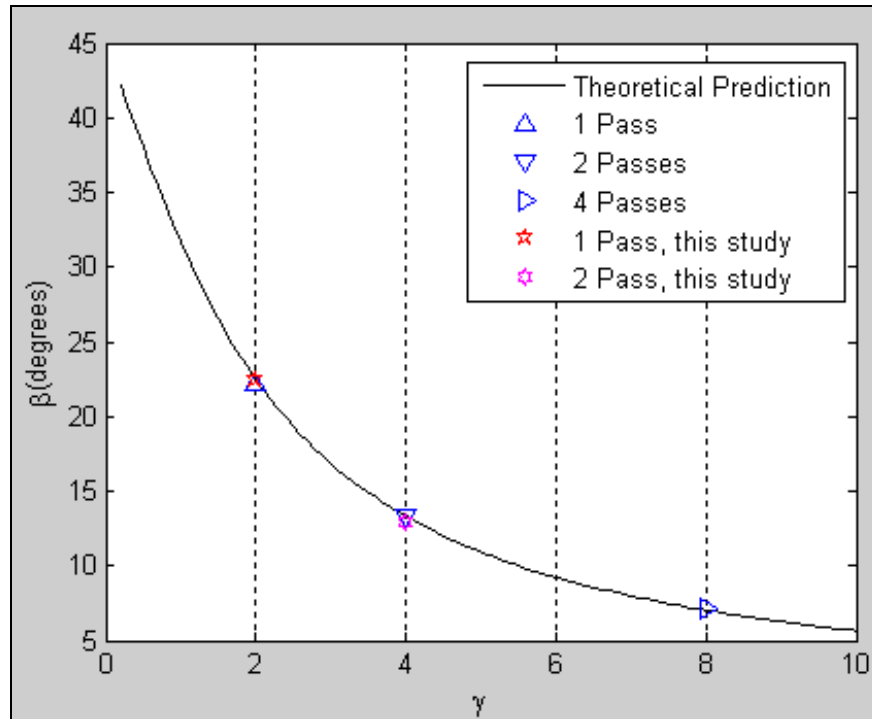
Figure 26    Predicted model for long-axis inclination angle versus shear strain superimposed with summary of empirical data. Theoretical Prediction line, and base one-, two-, and four-pass data (From: [10]).

## B.    AA6061

### 1.    Optical Micrographs

Optical micrographs in Figure 27 show the grain structure of AA6061-O prior to pressing. The sample was sectioned from an extruded, square bar; an elongated microstructure is seen on what will become the top and flow planes. The wavy boundaries between the grains in the flow plane should be noted, as this feature becomes significant upon pressing. Figure 28 and Figure 29 show the grain structure at higher resolution, revealing subgrains ranging from approximately 5 to 15 microns in size. Fine magnesium-silicide particles, due to precipitation in overaging of the material, can be resolved, along with the larger iron-silicide particles, that arise from presence of iron and silicon impurities.

Returning to Figure 27, the cross plane shows a transverse section of the grains revealing  thick, darkly etched grain boundaries dividing the grains.



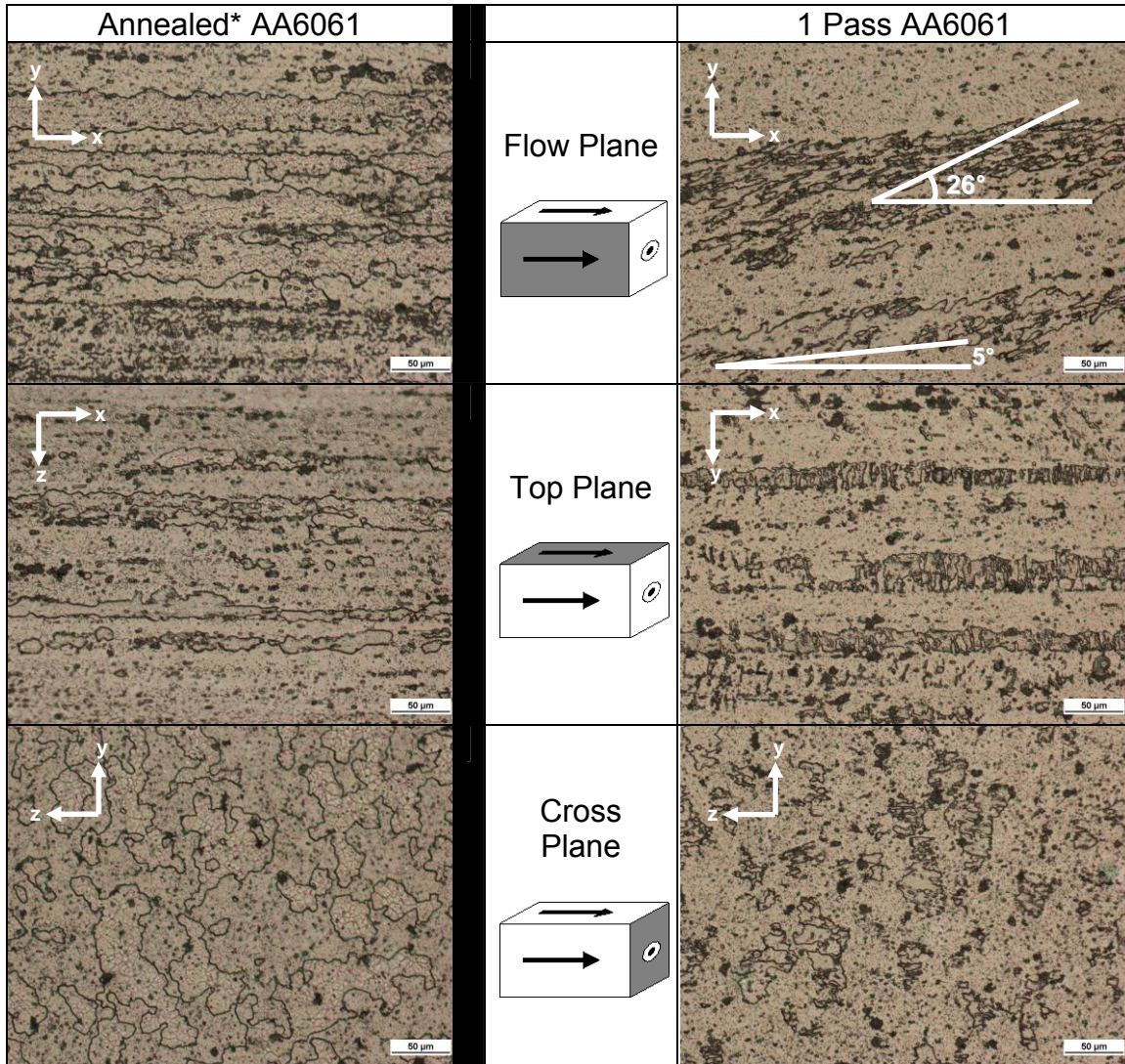| Annealed* AA6061 | | 1 Pass AA6061 |
|---|---|---|
| | Flow Plane | |
| | Top Plane | |
| | Cross Plane | |

Figure 27   Optical Micrographs of AA6061 on three orthogonal planes for the annealed, condition and one-pass samples
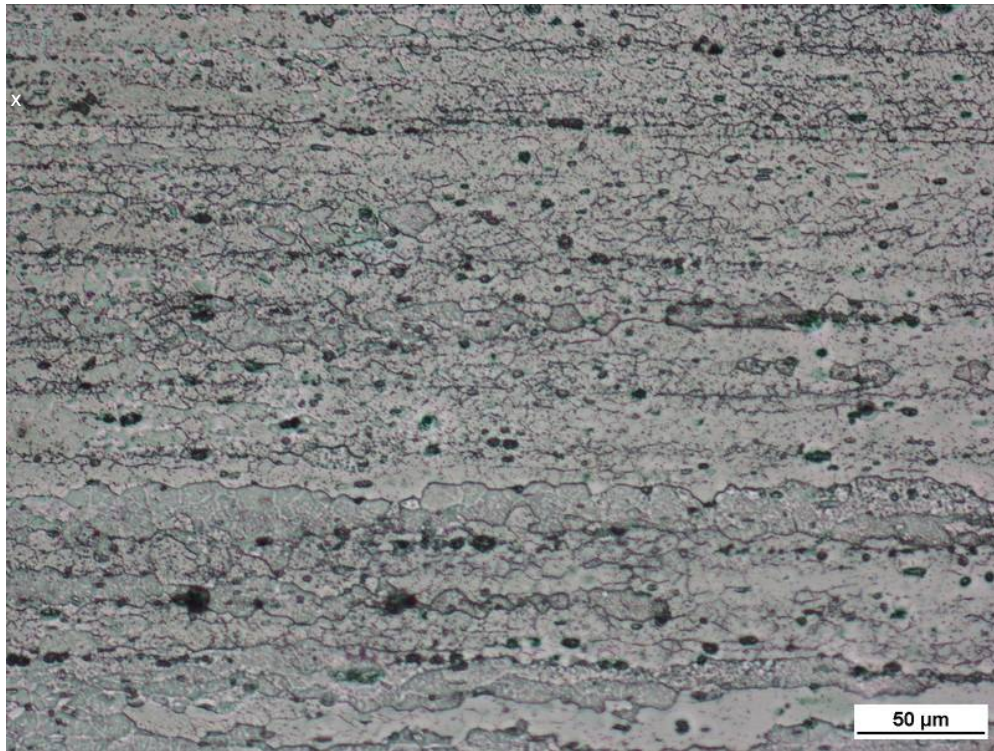
Figure 28    Higher    Magnification    of    AA6061-O    along    the    flow    plane
delineating grain structure



Figure 29    Highest magnification of AA6061-O along the flow plane

The results of one ECAP pressing are also shown in Figure 27. There are two noteworthy features on the flow plane image. First, the elongated grains appear to have a long axis inclined at ~5° with respect to the extrusion direction (x-axis). The aspect ratio for the initial grains was estimated to be 5 to 10, or perhaps greater. This angle of 5° is slightly higher than the model prediction depicted in Figure 7, for such a range of aspect ratio. This discrepancy will be addressed shortly.

Further, the wavy high-angle boundaries are no longer wavy—they all appear to become serrated and the serrations are aligned at a measured angle of 26° with respect to the extrusion direction. A possible explanation for this pertains to the existence of the subgrains. While the high-aspect-ratio grains are shearing, as expected, and becoming oriented at a small angle with respect to the billet axis, the subgrains, being equiaxed within the grain, shear according to the aforementioned model for equiaxed grains.

Figure 30 depicts a schematic representative of an equiaxed subgrain inscribed into an elongated grain having an aspect ratio of 10:1.5. Both are shown after one pass. Note that the spherical subgrain's major axis becomes inclined at 22.5°, while the major axis of the ellipsoidal grain is inclined only at 2.5° (both with respect to the extrusion direction, i.e. the x-axis). However, one should notice that the serrated edges are not inclined at the predicted 22.5°; they are inclined at 26°.
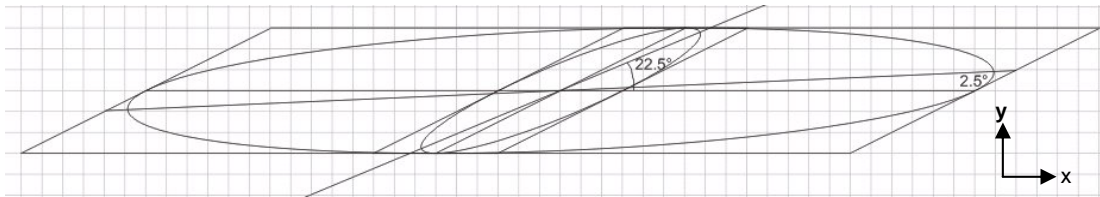


Figure 30   Model of an equiaxed subgrain inscribed in an elongated grain after one ECAP pass

Figure 31 summarizes the empirical results for both the elongated grains (m>>1) and equiaxed subgrains (m=1) as compared to theoretical predictions.

Clearly, both data points are shifted up, presumably by as much as 3.5° (26°-22.5°).  For a shear strain of two, a plot of the inclination angle versus aspect ratio, as depicted in Figure 32, reveals that an inclination angle of 5° would correspond to an aspect ratio, m, of slightly less than five.  This seems low in consideration of the optical imaging results.  However, if that angle were indeed 3.5°, a slightly more reasonable value for aspect ratio of 8-9 is achieved.  Careful analysis and measurements need to be made at these small angles, however, as the plot reveals there is a large increase in aspect ratio as the inclination angle drops below one.  Therefore, careful determination of prior grain size using image splicing and meticulous angle measurements need to be made in future experimentation, along with acquisition of significant amounts of data to minimize statistical error.
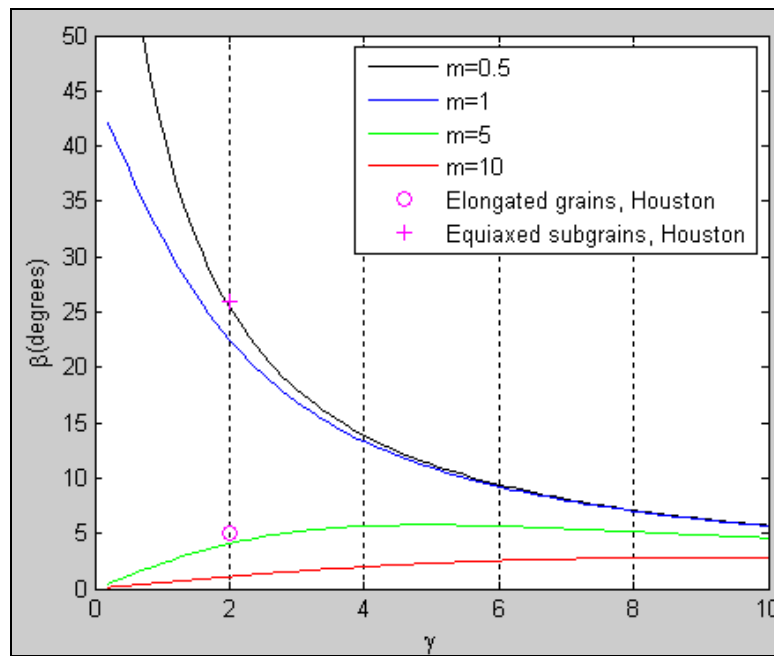


Figure 31    Summary of one-pass, route A, elongated and subgrain angles of inclination results superimposed on theoretical prediction plot (From: [10])
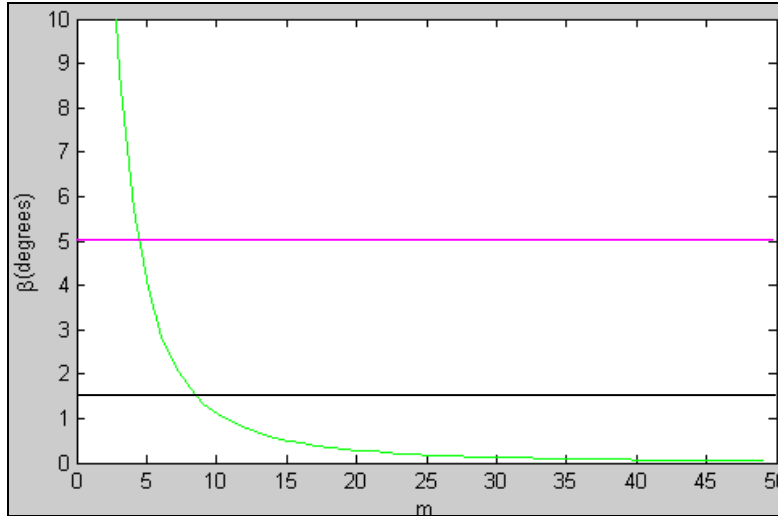
Figure 32   Inclination angle of long axis for $\gamma$=2 versus aspect ratio, m

The discrepancy in the angle results may be explained by looking at the actual pressing operation.   This particular sample, among other AA6061 samples, exhibited a curling phenomenon while going through the die exit channel.   Figure 33 below shows a clear gap on the top near the center and a clear gap on the end at the bottom indicating that the sample bowed as it left the relieved die exit channel.   This bowing would increase the apparent angles seen in both optical and orientation imaging results.
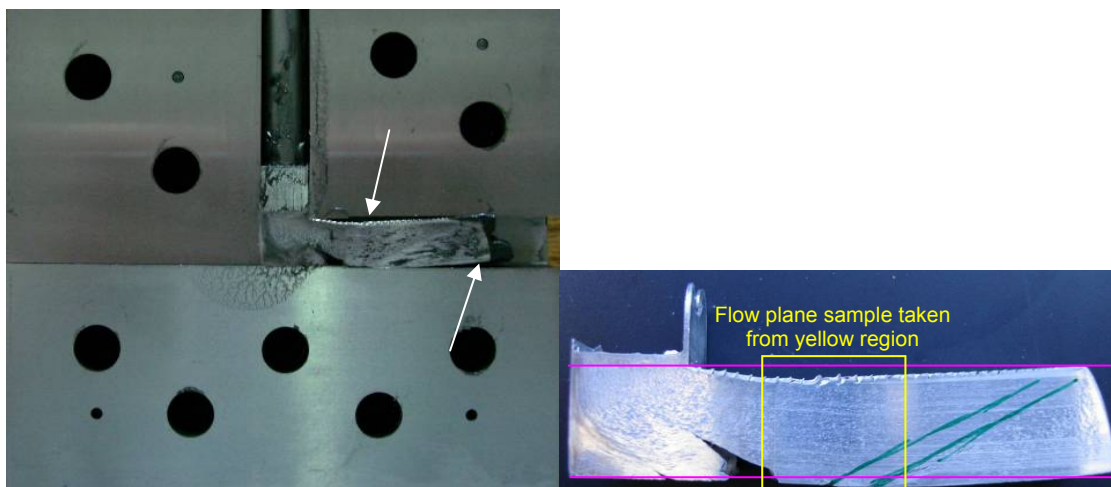


Flow plane sample taken from yellow region

Figure 33   AA6061 one-pass sample curling

43

If determination of the inclination angles of the grains upon exiting is deemed critical, then curling of the billet at the exit may be a significant issue. Thus, a die design that minimizes this curling should be considered.

The top plane results are as expected. The grain structure remains fundamentally the same, with the same dimensions, albeit with roughening of the grains due to shear bands. This clearly shows that the shear bands follow a preferential orientation, indicating that deformation is easier in some grains than others. The cross plane results are inconclusive as to whether compression has taken place; however, the overall grain shape remains intact along with the appearance of shear bands once again.

Figure 34 shows the optical micrograph results on the three orthogonal planes for two passes by route C of the AA6061. In the flow plane, there are no longer serrations at a preferential angle. Less differentiation can be seen between grains. The downward sloping angle is likely a result of the sample curling down as it passed through the die exit channel, similar to the previous discussion. The top plane remains once again intact in terms of general grain shape.

| | 2 Pass Route C AA6061 |
|---|---|
| Flow Plane |  |
| Top Plane |  |
| Cross Plane |  |
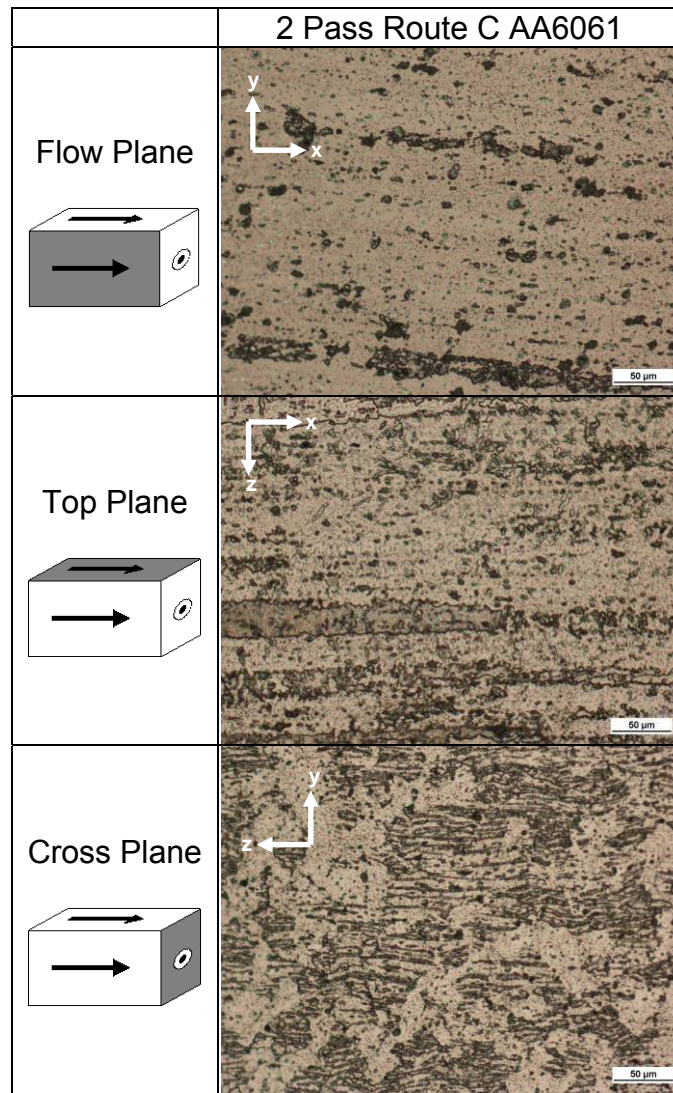
Figure 34  Optical Micrographs of AA6061 on three Orthogonal planes for the two-pass route C sample

## 2.    Orientation Imaging Results

The OIM results that are of most value consist of the flow plane Inverse Pole Figure Maps and Image Quality Maps which are shown in Figure 35.  The annealed 6061 sample shows a clear two-component fiber texture with the [100] fiber appearing in blue and the [111] fiber appearing in red (which may explain

darker and lighter regions seen in the optical images of Figure 33 and Figure 34). The 8° misalignment is inconsistent with the optical results and should be further investigated.

The one pass sample shows an inclination of the microstructure to be 27.5° with respect to the extrusion direction (x-axis). This is similar to the result of 26° achieved in optical microscopy in Figure 33 for the serrations along the grain boundaries. This further amplifies the possibility of the role of subgrains in the microstructure, as previously discussed. The low angle boundaries indicative of the subgrains are indicated by the subtle variations of the same basic colors—pink or cyan. The Inverse Pole Figure (IPF) shows a preferred texture.

The two-pass, route C sample shows some preferential orientation of the texture, as evidenced by the Inverse Pole Figure (IPF), but is different from both the initial annealed material and the one pass sample. No evidence of elongation or preferred angle of orientation with respect to the extrusion direction can be discerned.

Similar to the Image Quality Maps (IQM's) seen for AA1050, the AA6061 IQM's also appear to be indistinguishable with respect to each other (although a route A sample is not available for comparison at this time).
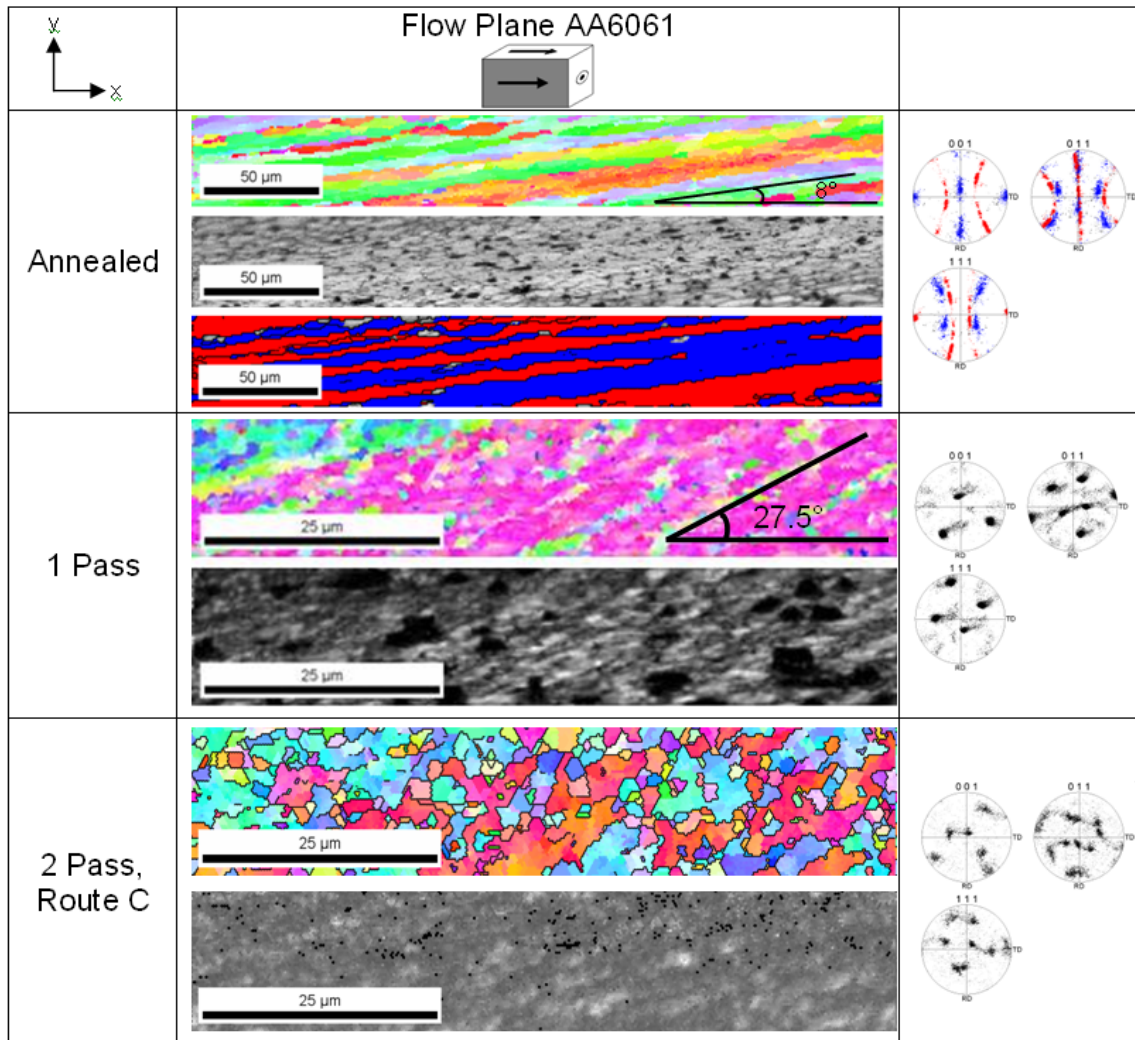
Figure 35   IPF and Image Quality Maps for AA6061 along the flow plane for annealed, one-pass, and two-passes via route C material

### 3.    Annealing Study Results

Figure 36 summarizes the results of an annealing study conducted at 450°C as a function of time to assess recrystallization and grain growth.   Two data points per sample were taken from different locations.   The grain size remained roughly constant throughout this study, implying that grain growth has already occurred within six minutes or less.   The IPF maps in Figure 37 indicate a random texture with some evidence of previous preferred orientation.
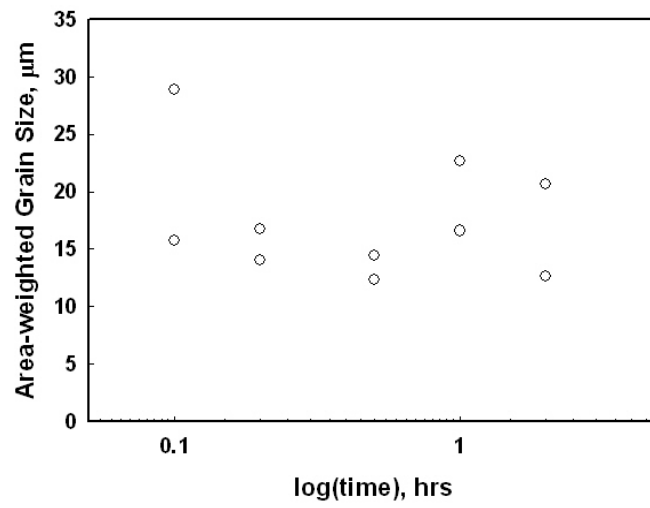
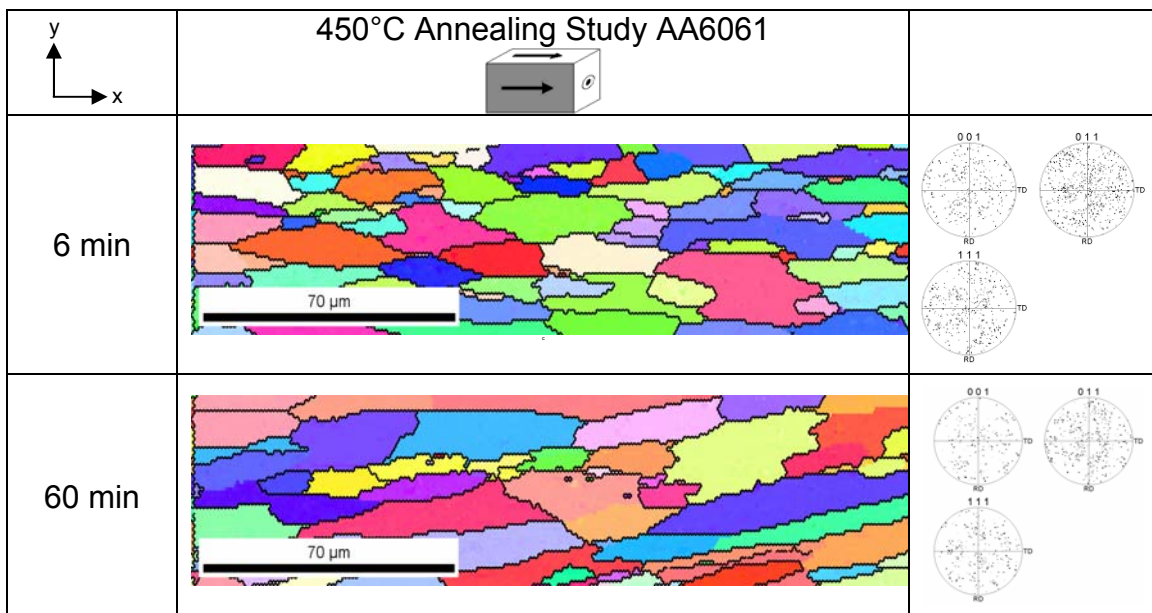Figure 36   Annealing Results for Grain Size as a Function of Time at 450°C



Figure 37   IPF Maps for 450°C Annealing Study

48

Since the temperatures were excessive in the previous study to determine the recrystallization temperature, a second study was performed with samples annealed for one hour at 250, 350, and 450°C. A period of one hour was chosen because it is the typical duration of an elevated temperature tension test, which is to be pursued in later research.

The results are shown in Figure 38 and Figure 39. As the IPF map depicts, there is still a preferential texture orientation as evidence of the onset of recrystallization. Since the material is not fully recrystallized, it cannot constitute a data point on the fully recrystallized grain size plot. However, as the IPF map indicates, at 350°C, the sample is fully recrystallized as evidenced by the random texture. The average grain size was measured to be 13 microns in two different locations.
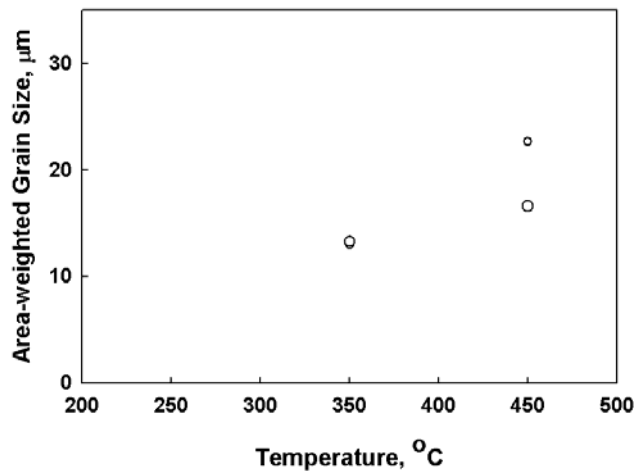


Figure 38  Grain Size as a Function of Temperature for a 1-hour Annealing Study
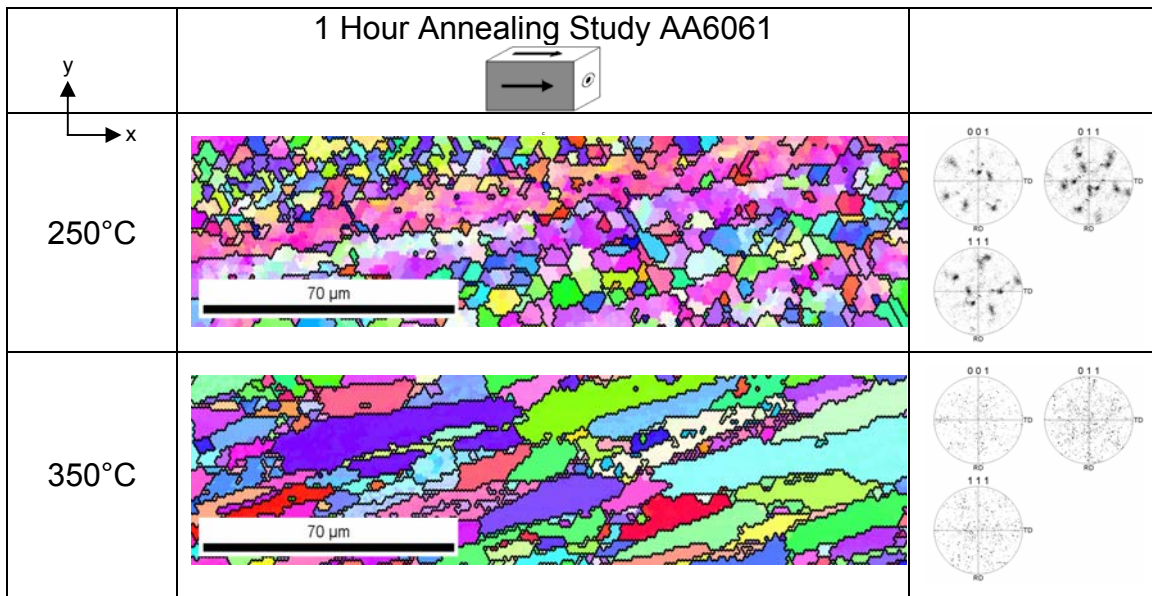
49

| | 1 Hour Annealing Study AA6061 | |
|---|---|---|
| y ↑ →x |  | |
| 250°C |  70 µm |  |
| 350°C |  70 µm |  |

Figure 39   IPF Maps of the 1-hour Annealing Study

## 4.      Conclusions and Recommendation for Further Work with AA6061

Ultimately, the goal of the overall program is to improve the formability of AA6061 by grain refinement.  At minimum, it is expected that grain sizes of 1-10 µm need to be achieved, which will require more than just two ECAP pressings followed by recrystallizing anneals.   The following experiments should be pursued:

- Pressing of AA6061 billets with elongated grains transverse to the billet length (aspect ratio>1), as suggested by Garcia-Infanta, *et al.* should be attempted to determine if this method indeed enhances grain refinement over those with aspect ratios greater than unity [10].

- The effects of Route $B_c$ should be considered when a more robust die has been fabricated.

- Properties achieved in the various strain paths should be compared to test the assertion made by Vinogradov, *et al.* that, despite differences in grain morphology and texture for different pressing routes, strain path had only minor effects on strength; however a greater influence on ductility was observed [32].

- With additional pressings, more annealing studies should be conducted, as the recrystallization temperature is expected to decrease due to the increased strain energy introduced.

- Once an optimum recrystallization temperature is found, with a promising grain size, hardness and ductility studies at both room- and elevated-temperatures should be done.

- Post-ECAP rolling should also be considered, as it has been shown to assist in superplasticity in an Al5154 alloy after only 4 ECAP passes to achieve elongation of 812% at initial strain rates of $5 \times 10^{-3}$/s [33, 34].

THIS PAGE INTENTIONALLY LEFT BLANK

# LIST OF REFERENCES

[1]  V.M. Segal, V.I. Reznikov, A.E. Drobyshevskiy, V.I. Kopylov.  Russian Metall., 1981, vol. 1, p. 99.

[2]  E.O. Hall, Proc Roy Soc B, 1951, vol. 64, p. 747.

[3]  N.J. Petch, Iron Steel Inst., 1953, vol. 174, p. 25.

[4]  R.Z. Valiev, T.G. Langdon, Prog. Mater. Sci., 2006, vol. 51, pp. 881-981.

[5]  R.Z. Valiev, Nature Mater., 2004, vol. 3, pp. 511-516.

[6]  Y. Iwahashi, Z. Horita, M. Nemoto, T.G. Landon, Acta Mater., 1998, vol. 46, pp. 3317-3331.

[7]  W.Q. Cao, S.H. Yu, Y.B. Chun, Y.C. Yoo, C.M. Lee, D.H. Shin, S.K. Hwang, Mater. Sci. and Eng. A, 2005, vol. 395, pp. 77-86.

[8]  Y.H. Zhao, X.Z. Liao, Z. Jin, R.Z. Valiev, Y.T. Zhu, Acta Mater., 2004, vol. 52, pp. 4589-4599

[9]  J.M. Garcia-Infanta, S. Swaminathan, A.P. Zhilyaev, F. Carreno, O.A. Ruano, T.R. McNelley, Mater. Sci. Eng. A, 2007, in press.

[10]  J.M. Garcia-Infanta, S. Swaminathan, F. Carreno, O.A. Ruano, T.R. McNelley.  Scripta Mater., 2008, vol. 58, pp. 17-20.

[11]  A.A. Salem, Z. Horita, T.G. Langdon, T.R. McNelley, S.L. Semiatin, Ultrafine Grained Materials III, ed. Y.T. Zhu, T.G. Langdon, R.Z. Valiev, S.L. Semiatin, D.H. Shin, T.C. Lowe (The Minerals, Metals and Materials Society TMS), 2004, pp. 1-8.

[12]  N. Hansen, X. Huang, D.A. Hughes, Ultrafine Grained Materials II, ed. Y.T. Zhu, T.G. Langdon, R.S. Mishra, S.L. Semiatin, M.J. Saran, T.C. Lowe (The Minerals, Metals and Materials Society TMS), 2002, pp. 3-14.

[13]  A to Z of Materials, Aluminum Alloy 6061, http://www.azom.com/details.asp?ArticleID=3328. Accessed December 1, 2007.

[14]  W.J. Kim, J.K. Kim, T.Y. Park, S.I. Hong, D.I. Kim, Y.S. Kim, J.D. Lee, Metall. and Mater. Trans A, 2002, vol. 33, pp. 3155-3164.

[15] C. Xu, M. Furukawa, Z. Horita, T.G. Langdon, Acta Mater., 2003, vol. 51, pp. 6139-6149.

[16] P.K. Chaudhury, B. Cherukuri, R. Srinivasan, Mat. Sci. Eng. A, 2005, vol. 410-411, pp. 316-318.

[17] K. Nakashima, Z. Horita, M. Nemoto, T.G. Langdon, Acta Mater., 1998, vol. 46, pp. 1589-1599.

[18] I.P. Semenova, G.I. Raab, L.R. Saitova, R.Z. Valiev, Mater. Sci. Eng. A, 2004, 387-389, pp. 805-808.

[19] S.D. Terhune, D.L. Swisher, K. Oh-ishi, Z. Horita, T.G. Langdon, T.R. McNelley, Metal. and Mater. Trans. A, 2002, vol. 33, pp. 2173-2183.

[20] K. Nakashima, Z. Horita, M. Nemoto, T.G. Langdon, Mater. Sci. Eng. A, 2000, vol. 281, pp. 82-87.

[21] M. Furukawa, Y. Iwahashi, Z. Horita, M. Nemoto, T.G. Langdon, Mater Sci. Eng. A, 1998, vol. 257, pp. 328-332.

[22] Y. Iwahashi, J. Wang, Z. Horita, M. Nemoto, T.G. Langdon, Scripta Mater., 1996, vol. 35, pp. 143-146.

[23] ASM Materials Handbook Volume 4: Heat Treating, Ninth Edition, p. 708.

[24] J.E. Shigley, C.R. Mischke: Mechanical Engineering Design, Fifth Edition, McGraw-Hill, 1989, pp. 328-349.

[25] R.K. Roy, S. Das. Journal of Mater. Sci., 2006, vol. 41, pp. 289-292.

[26] ASM Materials Handbook Volume 9: Metallography and Microstructures, Ninth Edition, 1985, pp. 354-355.

[27] A.P. Zhilyaev, K. Oh-Ishi, G.I. Raab, T.R. McNelley, TMS, Warrendale, PA, 2006, pp. 113-118.

[28] A.A. Salem, T.G. Langdon, T.R. McNelley, S.R. Kalidindi, S.L. Semiatin, Metall. and Mater. Trans. A, 2006, vol. 37, 2879-2891.

[29] S. Ferrasse, V.M. Segal, K.T. Hartwig, R.E. Goforth, Metall. Mater. Trans. A, 1997, vol. 28, pp. 1047-1057.

[30] Y. Iwahashi, M. Furukawa, Z. Horita, M. Nemoto, T.G. Langdon, Metall. Mater. Trans. A, 1998, vol. 29, 2245-2252.

[31]   A. Gholinia, P.B. Pragnell, M.V. Markushev, Acta Mater., 2000, vol. 48, 1115-1130.

[32]   A. Vinogradov, T. Ishida, K. Kitagawa, V.I. Kopylov, Acta Mater., 2005, vol. 53, pp. 2181-2192.

[33]   K.T. Park, H.J. Lee, C.S. Lee, W.J. Nam, D.H. Shin, Scripta Mater., 2005, vol. 51, pp. 479-483.

[34]   K.T. Park, H.J. Lee, C.S. Lee, D.H. Shin, Mater. Sci. Eng. A, 2005, vol. 393, pp. 118-124.

THIS PAGE INTENTIONALLY LEFT BLANK

# INITIAL DISTRIBUTION LIST

1.  Defense Technical Information Center
    Ft. Belvoir, Virginia

2.  Dudley Knox Library
    Naval Postgraduate School
    Monterey, California

3.  Dr. Joan Fuller
    Air Force Office of Scientific Research (AFOSR)
    Arlington, Virginia

4.  Dr. Tony Healey
    Naval Postgraduate School
    Monterey, California

5.  Prof. Terry McNelley
    Naval Postgraduate School
    Monterey, California

6.  Dr. Srinivasan Swaminathan
    Naval Postgraduate School
    Monterey, California

7.  Dr. Jianqing Su
    Naval Postgraduate School
    Monterey, California

8.  S.L. Semiatin
    Air Force Research Laboratory
    Wright-Patterson AFB, Ohio